Top Curr Chem (2010) 293: 115–153
DOI 10.1007/128_2009_7

Published online: 26 August 2009

Chiral Metal-Organic Porous Materials: Synthetic Strategies and Applications in Chiral Separation and Catalysis

Kimoon Kim, Mainak Banerjee, Minyoung Yoon, and Sunirban Das

Abstract In the light of growing demand for chiral purity in biological and chemical processes, the synthesis of chiral metal-organic porous materials (CMOPMs) have become immensely important because of their potential applications in chiral separation and asymmetric catalysis. In this chapter, the synthetic strategies for CMOPMs are discussed briefly keeping the focus on their applications. Two distinct approaches have been taken to synthesize a wide variety of chiral structures with different topologies and accessible cavities. Several CMOPMs have shown catalytic activity and enantioselectivity toward a number of chemical transformations. On many occasions, the chiral pores of the MOPMs have been utilized in order to achieve separation of enantiomers from racemates. Recent applications of homochiral MOPMs in heterogeneous asymmetric catalysis and chiral separations are also presented here.

Keywords Asymmetric catalysis • Chirality • Crystal structure • Enantioselection • Metal-organic porous materials

K. Kim (✉), M. Banerjee, M. Yoon and S. Das
Department of Chemistry, Division of Advanced Materials Science, and
National Creative Research Initiative Center for Smart Supramolecules,
Pohang University of Science and Technology, Pohang, 790-784,
Republic of Korea
e-mail: kkim@postech.ac.kr

Contents

Abbreviations

1,2-pd	1,2-propanediol
asp	aspartate
bdc	1,4-benzenedicarboxylate
BINAP	2,2′-bis(diphenylphosphino)-1,1′-binaphthyl
BINOL	2,2′-dihydroxy-1,1′-binaphthyl
bipy	4,4′-bipyridine
bpdc	4,4′-biphenyldicarboxylate
bpe	1,2-bis(4-pyridyl)ethylene
bpy	2,2′-bipyridine
btc	1,3,5-benzenetricarboxylate
CMOPM	Chiral metal-organic porous material
CSP	Chiral stationary phase
dca	dicyanamide
DPEN	1,2-diphenylethylenediamine
IRMOF	Isoreticular metal organic framework
lac	Lactate
MOF	Metal-organic framework
MOPM	Metal-organic porous material
pic	picoline
QA	6-methoxyl-(8*S*,9*R*)-cinchonan-9-ol-3-carboxylate
sala	*N*-(2-hydroxybenzyl)-L-alanine
salen	1,2-cyclohexanediimino-salicylidene
SBU	Secondary building unit
SHG	Second harmonic generation
TOF	Turn over frequency
TON	Turn over number
UHP	Urea hydroperoxide

1 Introduction

Porous materials are ubiquitous in nature. The earth's crust contains many porous materials e.g., soil, sandstones, carbonates, shales; even biological tissues can be porous. Porous materials have found enormous applications in many traditional scientific fields such as catalysis, adsorption, and environmental technology because of their high surface area coupled with many other unique chemical and physical properties. A classic example of naturally occurring porous materials is zeolites, a class of aluminosilicates with interconnected small cavities of 4–13 Å in dimensions, used as catalysts for oil refining, petrochemistry, and organic synthesis in the production of fine and specialty chemicals [1]. The loosely bound cations present inside the channels and pores of zeolites can be readily exchanged with other cations when in aqueous media; this also make them ideal choices as water softening devices and in detergent and soap industries. In fact, a major part of the global economy (~$350 billion) is currently based on the use of crystalline microporous zeolites in several industrial processes [2], which reflects the importance of such porous materials in the daily life of man.

As the demand for optically pure compounds grows, significant research efforts have been devoted to developing chiral zeolites and related chiral porous solids with the goal of using them for the production of enantiopure materials via asymmetric chemical transformations and/or chiral separations [3]. Despite considerable efforts, however, only a few optically *pure* zeolites have been synthesized to date [4,5]. More importantly, local chirality at the catalytic center would provide more impact than the topological chirality in imparting strong asymmetric induction to the substrate during the reaction. This has prompted exploration of other strategies for the synthesis of similar porous solids with embedded chiral functionalities, which may find practical applications in chirotechnology.

There has been considerable research interest in metal-organic porous materials (MOPMs) or metal-organic frameworks (MOFs) over the last couple of decades because of their potential impact on several technologies, such as gas storage, separation, and heterogeneous catalysis [6–11]. Although not as robust as zeolites, they certainly have some advantages over zeolites. MOPMs are typically synthesized under very mild conditions, which should allow facile construction of homochiral MOPMs by appropriate choice of chiral building blocks. Ideally, they can possess chiral functionalities that are accessible via the open channels or cavities. Such readily accessible, regularly ordered chiral functionalities could be exploited to generate heterogeneous asymmetric catalysts for the economical production of optically pure compounds. The cavities of homochiral MOPMs can also be utilized in separation of enantiomers by selective recognition/sorption. Successful design of homochiral MOPMs may therefore lead to practical applications in the field of chirotechnology. From the beginning of this century, research of great potential in this field has started to flourish. Several review articles on this highly important field of research are available [12–14]. This review aims to provide current status and trends in the development of chiral metal-organic porous materials (CMOPMs)

and indicate their useful and practical applications in the burgeoning field of chirotechnology.

1.1 Chirality in Crystal Structure

In the context of chemistry, the term "*chirality*" usually refers to a pair of molecules that cannot be superimposed onto each other - also referred to as enantiomers or optical isomers. The main characteristic of chirality is the absence of an axis of improper rotation. The existence of such a symmetry element is implied by the presence of either a mirror plane through the central atom or a center of inversion; if either of these elements is present, the molecule is achiral. The chiral sense of a molecule is specified by its absolute configuration (*R/S*, D/L, or Δ/Λ). Molecules may be present as enantiomeric mixtures, of which those with compositions 100:0 and 0:100%, described as enantiomerically pure or homochiral, and the equimolar one of 50:50% described as a racemate or racemic mixture are particularly important.

A total of 230 space groups, which are the combination of 32 crystallographic point groups and 14 Bravais lattices, are used to define the 3D solid-state structure of a molecule. Out of these 230 space groups, 65 are noncentrosymmetric, which contain only pure rotation and screw axes- for example, the two-, three-, four-, or six-fold rotations with screw axis without any plane of symmetry or inversion center. Among these, 22 space groups are pair wise enantiomorphous, and therefore inherently chiral. Within each pair, inversion through a point transforms one space group into the other, e.g., $P6_2$ transforms into $P6_4$ and vice versa. When coordination polymers crystallize, they form well-ordered 1D, 2D or 3D net structures connected through covalent or noncovalent bonds with defined topologies. Coordination polymers with chiral components always crystallize in noncentrosymmetric space groups due to the embedded chirality in the subunits. However, in principle, a crystal with single-handed helical arrangement of the components is chiral. Therefore, a helix may be a good model to transmit chirality to the crystal structure even if it is constructed from achiral components. In this sense, the topology-based approach is much more convenient for the design of noncentrosymmetric coordination networks because of the presence of some inherently chiral nets. The simplest and most common nontrivial regular 3D chiral topologies are 3-connected (10, 3)-a and (12, 3) nets (Fig. 1) [15]. The symbol (10, 3) is used to characterize the topology of a net in which all nodes are 3-connected and the shortest circuits involving all three different pairs of connections radiating from each node are 10-gons. The chirality in (10,3)-a arises from the disposition of the same handed 4-fold helices parallel to each of the three crystallographic cubic axes. Similarly, a (12,3) net can be realized in a completely strain-free manner from alternating T and trigonal nodes. Among 4-connected nets, diamond-like nets with unsymmetrical linkers have the ability to generate noncentrosymmetric crystals. The diamondoid network consisting of alternating adamantane-like cavities can be constructed with alternate tetrahedral metal centers linked together by rigid, linear bridging ligands (Fig. 1c).

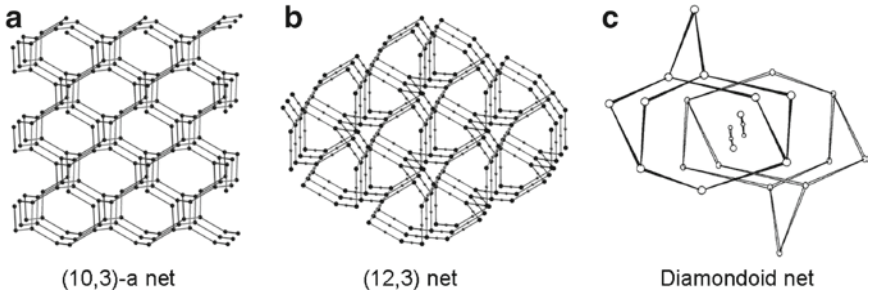

Fig. 1 Representative topologies of (10,3)-a, (12,3), and 2-fold diamondoid nets

1.2 Metal-Organic Porous Materials: Brief History and Key Developments

There are a number of excellent reviews on coordination polymers, MOFs or MOPMs [9–11,16–20]. Here we briefly touch the history and key developments in this area.

The design of extended solids with ordered array of the basic building units has been a subject of intense study in conjunction with developing new solid-state functional materials. Hydrogen bonding has been extensively used in designing organic solids with specific structures, largely because of its strength and directionality [21–23]. The strong and yet reversible nature with high directionality of metal-ligand coordination bond makes it widely exploited in constructing network structures with specific topologies and geometries. In 1990, for the first time, Robson introduced a design concept to the construction of 3D MOFs using appropriate molecular building blocks and metal ions [24]. Following the seminal work, several groups including Zaworotko [25,26], Yaghi and O'Keeffe [27,28] contributed significantly to the developments in this field in terms of establishing designing principles. Particularly, the node (simple metal ions or metal clusters) and spacer (bridging organic ligands) approach has been remarkably successful in producing well-ordered crystalline solids with predictable network architectures [29].

In particular, MOFs with large pores or metal-organic porous materials (MOPMs) have attracted considerable attention due to their potential applications in many areas including gas storage and catalysis. Considerable efforts have thus been made in designing MOPMs with specific pore sizes, shapes, and chemical environments. One of the early issues in this area was to design a stable framework. MOFs are usually produced with guest molecules – typically solvents or templates – in the pores. However, the attempts to remove guest molecules from the pores often result in collapse of the framework. Therefore, rigid and directional building units are the prime choice in controlling the porosity as well as the stability of the frameworks. Yaghi and coworkers demonstrated how the concept of secondary building units (SBUs) could be applied with great success to design highly porous and stable rigid MOFs [30–32]. The clusters of metal-carboxylates have been used

as rigid SBUs that act as vertices in the framework, and the length of the organic linkers can be modulated to vary the pore sizes systematically. With increasing pore size, however, frameworks show a tendency to undergo interpenetration. Although interpenetration may increase the stability of the framework and selectivity in sorption, it substantially decreases the possibility to accommodate larger molecules for separation and catalysis. The use of bulky solvent molecules as a template or bulky ligands at times decreases the possibilities of interpenetration [33].

The primary objectives of the design and synthesis of these open-framework solids are to utilize them as functional materials. Except some applications such as nonlinear optics, many applications including catalysis, ion exchange, and gas sorption rely on the fact that the open cavities allow passage of certain species to the active centers and exclude others [34–36]. The basic functions of these materials, whether two- or three-dimensional, are dependent on the building blocks and topology of the material. With the achievement of permanent porosity and high surface area, these materials are used for gas storage and separation. For example, Kitagawa and Yaghi first demonstrated the use of such materials for methane and hydrogen gas storage, respectively [37,38]. The guest induced structural transformations have also been used for selective sorption and separation [39]. However, one of the most exciting applications of MOPMs is catalysis. Fujita first elegantly demonstrated the use of MOPMs as a heterogeneous catalyst to facilitate chemical transformations, while Kim demonstrated that homochiral MOPMs are useful for enantioselective separation and catalysis [40,41].

1.2.1 Chiral Metal-Organic Porous Materials

A compelling motivation to prepare porous materials with built-in chirality is their potential use in enantioselective separation and in the synthesis of optically pure compounds, beside their second harmonic generation (SHG) properties. Although microporous zeolites show a profound range of applications in heterogeneous catalysis, the dearth of chiral zeolites limits their contribution in heterogeneous asymmetric catalysis or chiral separation. There are sporadic reports on the immobilization of chiral units in zeolites and successful application in asymmetric induction. However, this process does not guarantee a stable well-ordered chiral environment within the pores [42,43]. CMOPMs with well-defined chiral centers and/or reactive sites may thus emerge as a useful substitute to the practically inaccessible chiral zeolites in the realm of chirotechnology. Such chiral porous matrices have some additional advantages over zeolites. First, it is easy to introduce various functional groups into the cavity of CMOPMs. Second, these materials are not only restricted to the rigid tetrahedral network topologies like zeolites, but a variety of topologies can be generated with more internal flexibilities to allow easy access of guest molecules to the cavities. Third, it is also possible to keep hydrophilic and hydrophobic balance in the pores by judicious choice of linkers. During the last 5–10 years, several CMOPMs have been synthesized adopting different strategies, which will be discussed in Sect. 2 in detail.

2 Synthetic Strategies of Chiral MOPMs

To achieve well-ordered chiral catalytic centers in the solid phase, it is necessary to select proper chiral organic building units and metal salts that form periodically ordered porous materials with appropriate void space. The accessibility of the active sites, which depends on the shape and size of the window and cavity in the MOPM, is crucial for the activity and selectivity of the final catalyst. Nanometer sized pores are ideal to access the catalytic centers of the framework, and to achieve strong multidirectional interactions between substrates and the chiral environment of the cavities. Keeping these points in mind, different strategies have emerged for the construction of well-defined metal-organic porous frameworks with chiral environments. In principle, one can construct CMOPMs in two distinct ways, (a) by deliberate design of homochiral frameworks from the building blocks, and (b) introduction of chiral units inside pre-assembled achiral frameworks by post-modification. A large number of chiral MOPMs have been synthesized using the first approach, either from achiral building blocks or from chiral molecular components. In this section, we describe the strategies for the construction of CMOPMs with illustrative examples.

2.1 Direct Synthesis of Chiral MOPMs from Building Blocks

Chiral building blocks are the preferred choice for building homochiral frameworks. However, achiral molecular components are also capable of generating chiral frameworks by adopting chiral net structures. Both approaches are discussed here in separate subsections.

2.1.1 Chiral MOPMs from Achiral Building Blocks

Any MOPM - whether built with achiral or chiral components, may acquire a chiral space group during crystallization by unique spatial disposition of all the building units within the MOPM. There are numerous examples of MOPMs built with simple achiral molecules that crystallize in chiral space groups through self-resolution [44–47]. Although the individual crystals of such systems are chiral, the bulk samples tend to contain both enantiomorphs and thus can be racemic. However, it is not understood how to induce homochirality in the bulk phase in such a way that every crystal is oriented with the same chirality. Therefore, the design of noncentrosymmetric coordination networks requires identification of those nets that are not predisposed to pack in centrosymmetric space groups, and identification of potential nodes and spacers that can lead to the desired noncentrosymmetric topologies. To increase the possibilities of having control over the predicted topology, however, simple systems are better such as 3-connected (10,3)-a net, which is inherently

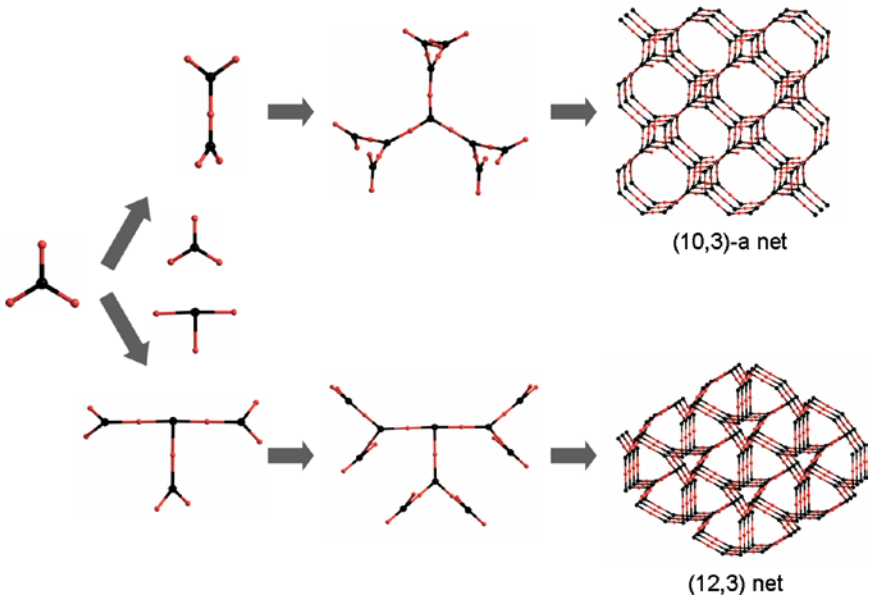

Fig. 2 The course of the assembly of 3D (10,3)-a and (12,3) nets from the 3-connected nodes and liner linkers

chiral (Fig. 2). Many researchers have tried to generate homochiral MOPMs with this topology through self-resolution. Although in some cases individual crystals were enantiomorphic by deliberate design, the bulk sample was still racemic [48,49]. Other networks with applicable porosity include 3-connected (12,3) and 4-connected diamond-like nets. There are several reports of chiral MOFs with these networks through proper selection of linkers, but the high propensity of higher-fold interpenetration often reduces the void space [31].

To generate bulk chirality, the two possible enantiomeric forms must be differentiated. This can be achieved by using chiral templates, such as enantiopure solvents of crystallization, counter cations, or auxiliary ligands. Rosseinsky and coworkers used optically pure coligand, 1,2-propanediol (1,2-pd) as a template to direct the formation of homochiral porous networks of the type $M_3(btc)_2$, where M is a divalent metal ion and btc is 1,3,5-benzenetricarboxylate [50]. In the doubly interpenetrated (10,3)-a network of $[Ni_3(btc)_2(py)_6(1,2\text{-pd})_3]\cdot 11(1,2\text{-pd})\cdot 8(H_2O)$, **1**, the coordinating 1,2-pd acts as a chiral coligand that controls the helical growth of all crystals in the same direction to afford homochiral materials. However, only the *S*-isomer of 1,2-pd binds to the metal center during the formation of the chiral framework. This selectivity was observed even when the crystals were grown from racemic diol, which was ascribed to the steric conflict between the methyl group of diol and btc unit. Recently, Morris and coworkers used a nonligating template to exert chiral purity on a framework [51]. They used chiral ionic liquid, 1-butyl-3-methylimidazolium L-aspartate, as a solvent as well as a template for the synthesis

of homochiral MOPM, $[(BMIm)_2][Ni(Hbtc)_2(H_2O)_2]$, **2**, where the bulky organic counter cations occupied most of the void space. Obviously, a synthetic approach that allows the achiral molecular precursors into extended homochiral frameworks, templated by enantiopure coligands or counter cations will help expanding the diversity of metal-organic homochiral solids. Removal of these extra framework species is, however, much more difficult than that of neutral solvent molecules to access the cavity or channel.

2.1.2 Chiral MOPMs from Homochiral Building Blocks

The most reliable and rational strategy to design homochiral MOPMs is the combination of metal or metal cluster (SBU) containing nodes and chiral organic ligands. The chiral organic ligands ensure the chirality in the final networks. The chiral organic ligands can be used in two ways to construct homochiral MOPMs: (a) using homochiral linkers to connect metal ions or SBUs, or (b) using enantiopure chiral auxiliary ligands to generate chiral SBU, which subsequently connect with rigid achiral linkers. In some cases, it is difficult to classify them into one of the two approaches, but we try to demonstrate the principle with illustrative examples.

From Homochiral Bridging Linkers

The use of well-defined and directional homochiral bridging ligands as building blocks for the synthesis of homochiral MOPMs is without any doubt the most reliable and promising strategy among all available strategies. Before the development of well-known "*reticular synthesis*" or predesigned SBU concept, commercially available, multitopic, homochiral ligands with the propensity to bridge metal centers such as amino acids or hydroxyacids were the most attractive choice for introducing homochirality into a MOF. For example, Randford and coworkers used the amino acid derivative, *N*-(2-hydroxybenzyl)-L-alanine (H_2sala), and metal ions for the synthesis of a homochiral MOF. A honeycomb like framework was formed through the propagation of hydrogen bonded helical chains of discrete dimer, $[\{Zn(sala)(H_2O)_2\}_2]$, **3** [52]. Although thermal dehydration retains the framework integrity, the accessible free space is very small. Subsequently, several other groups tried to generate chiral MOPMs with other cheap and readily available chiral ligands. In some cases, they showed moderate chiral separation; however, their structural prediction was found to be difficult because of the high order flexibility inherent in these building blocks. In addition, these ligands are not always equipped with functional groups required for chiral separation and asymmetric catalysis. Therefore, it is necessary to design rigid, homochiral ligands with proper functionality and connectivity and apply a modular approach to produce the desired framework (Fig. 3).

In 2000, Kim and coworkers reported the first example of a well-defined, crystalline, homochiral MOPM with catalytic activity [41]. They synthesized the

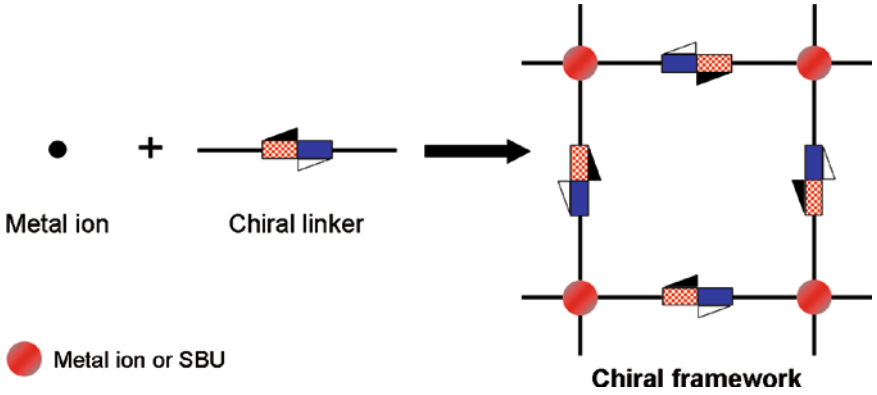

Fig. 3 Schematic representation of the general synthetic strategy of chiral framework by using chiral linker

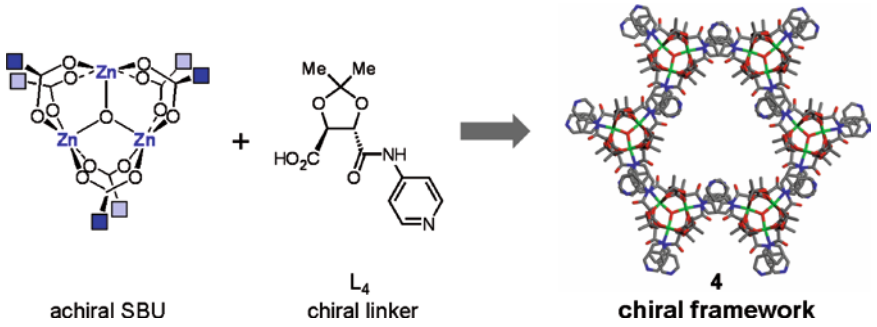

Fig. 4 Schematic representation of the synthesis of POST-1

homochiral open-framework solid, $[Zn_3(\mu^3\text{-}O)(L_4\text{–}H)_6]\cdot 2H_3O\cdot 12H_2O$ (referred to as POST-1 (**4**)) using enantiopure tartaric acid-based unsymmetrical ligand (L_4) (Fig. 4). In POST-1, oxo-bridged trinuclear zinc cluster behaved as an SBU, which in turn was interconnected to generate 2D infinite layers with large 1D channels. The ligand, L_4 can be considered semi-flexible, which leads to an interesting but 2D layered structure. However, more rigid, linear chiral linker, like BINOL or chiral salan based ligands, are expected to produce robust frameworks.

Lin and coworkers used rigid BINOL-based chiral ligands to synthesize several 2D or 3D homochiral MOPMs. The reason behind the selection of BINOL derivatives as chiral linker is their active involvement in several well-known homogeneous catalysts. In order to achieve larger pore size with predictable structure, they designed linear dicarboxylic acid functionalized BINOL derivative (6,6′-dichloro-2,2′-diethoxy-1,1′-binaphthyl-4,4′-dibenzoic acid), L_5, to link with zinc ion. As a result, a chiral framework of cubic topology, $[Zn_4(\mu^4\text{-}O)(L_5)_3(DMF)_2]\cdot 4DMF\cdot 3CH_3OH\cdot 2H_2O$ (**5**), with octahedral zinc-carboxylate unit, $Zn_4O(O_2C^-)_6$, as SBU was obtained [53]

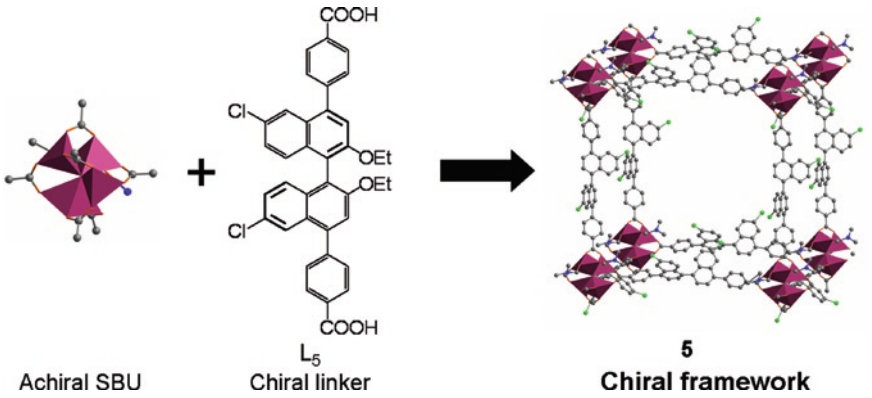

Fig. 5 A typical example of the synthesis of chiral framework by using rigid chiral linker (L_5) and achiral metal cluster SBU

(Fig. 5). Though they could isolate the product with desired network, the interpenetration led to almost closed-pack system. Later, through suitable selection of molecular building blocks and reaction condition, they synthesized a large number of chiral MOPMs with the same strategy.

More recently, Hupp and Nguyen used salen-based chiral Mn-complex as a chiral linker to generate chiral MOPM through pillaring with Zn-carboxylate paddlewheel [54]. Bu et al. also employed the same strategy to construct several homochiral open-framework materials using homochiral camphoric acid as a rigid linker [55].

From Chiral Secondary Building Units

The predesigned synthesis of CMOPMs with readily available chiral building blocks, such as amino acids or sugars, is very difficult as they are flexible in nature. However, these ligands can be utilized as auxiliary units to form clusters, 1D chains, or 2D layers, which function as chiral SBU to generate well-defined networks through proper selection rigid achiral linkers (Fig. 6). Recently, Kim and Fedin have described the synthesis of homochiral framework with permanent porosity by using chiral linear chain as SBU [56]. Homochiral L-lactic acid has been used to form a chiral 1D chain with zinc ion, which is in turn interconnected through 1,4-benzenedicarboxylic acid (H_2bdc) to afford a chiral 3D open-framework [Zn_2(bdc)(L-lac)(dmf)]·(DMF), (**6**·DMF) (Fig. 7). The medium-sized pores (~5 Å) thus formed are essentially chiral by the presence of L-lactate moieties. In a very similar approach, Rosseinsky used chiral 2D layers of Ni-(enantiopure-aspartate) as SBUs, to generate porous 3D homochiral frameworks by pillaring with appropriate neutral achiral bridging linkers [57].

So far, we have discussed several general strategies for constructing homochiral porous frameworks. However, additional requirements are necessary for them to be

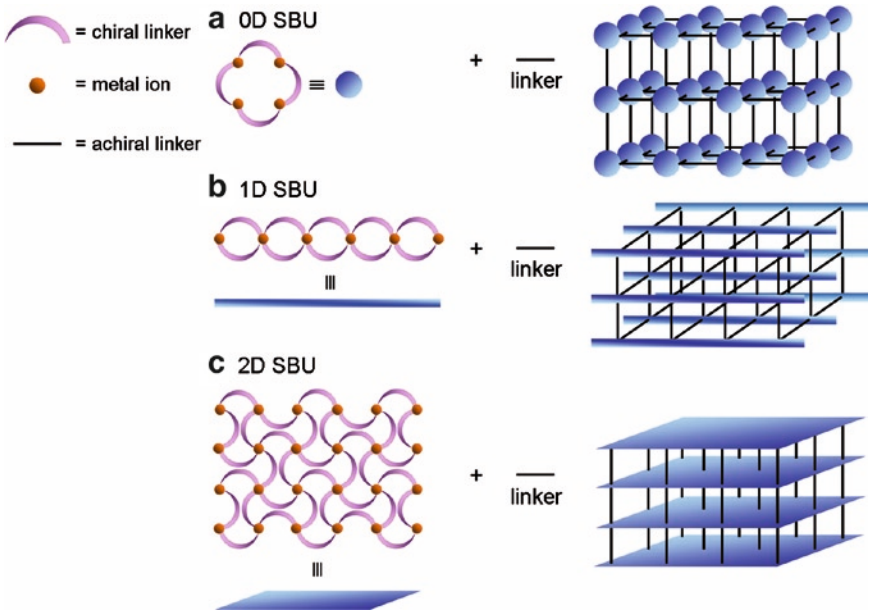

Fig. 6 A synthetic approach toward homochiral metal-organic frameworks through linking chiral secondary building blocks by achiral ligands

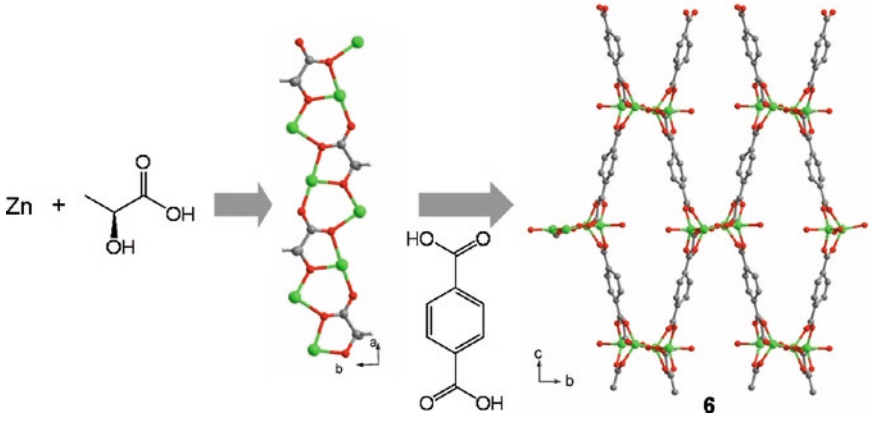

Fig. 7 The formation of 1D chain SBU by zinc ion and L-lactate and the construction of 3D network structure by achiral bridging ligand (viewed along *b* axis)

useful in enantioselective catalysis, including the presence of catalytic centers in the chiral pores.

The simplest system that behaves as a functional material in catalytic processes can be designed with a coordinatively unsaturated metal centers linked to a chiral

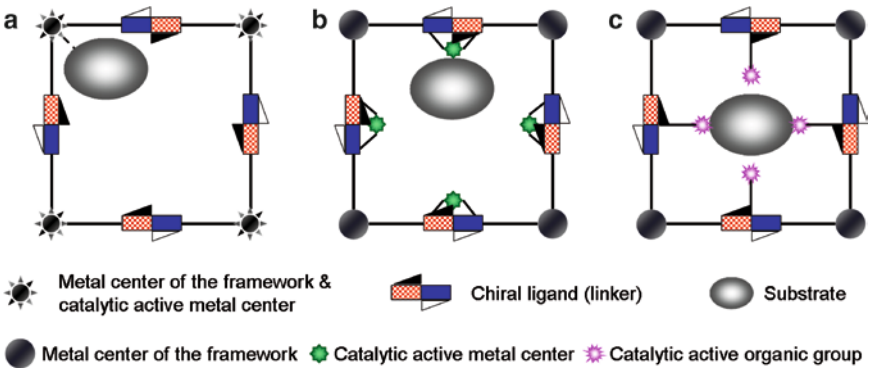

Fig. 8 Schematic representation of the synthetic approaches to possible chiral frameworks for catalysis and separation

ligand to construct a porous metal-organic assembly (Fig. 8a). Here, the metal centers in the homochiral metal-organic assembly should play a dual role as both the structural forming and the catalytically active centers, and the metal center should have an open coordination site or a readily removable ligand. In most cases however, the metal coordination sites are either fully occupied or sterically crowded, which leads to little or no catalytic activity. To avoid such difficulties, one may design a metal-organic assembly with one metal forming the framework, and another catalytically active metal open towards the pore (Fig. 8b).

Pendant organic subunits may also perform catalytic reactions (Fig. 8c) [41,58]. For example, a free basic functional group such as amine can perform a base catalyzed reaction inside the pore. However, for the asymmetric catalysis, the organic catalytic unit should itself be chiral or positioned near a chiral center in the pore.

2.2 Chiral MOPMs Through Postmodification

Unlike previous strategies, the postmodification approach does not require preparation of specific, intricate building blocks for the generation of a targeted functional MOPM. Indeed, MOPMs can be readily modified by subsequent reaction with a variety of organic molecules without changing the framework structure. Kim et al. [41] first successfully demonstrated the postsynthetic covalent modification of MOPMs by *N*-alkylation of the free pyridyl groups present in the cavities of POST-1 without altering the original 3D framework. In recent studies, Cohen and coworkers incorporated various organic subunits to the pendant amino group by postsynthetic covalent modification in IRMOF-3, which is otherwise impossible to introduce inside the framework [59,60]. More recently, Chang and Férey reported the incorporation of primary amine at the coordinatively unsaturated metal center by post-modification, which showed a catalytic activity in Knoevenagel condensation [61].

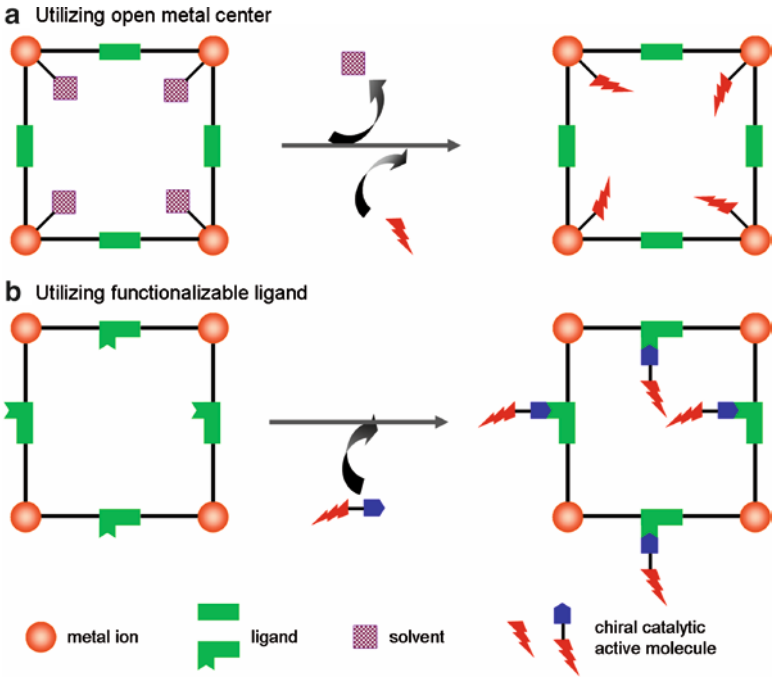

Fig. 9 Schematic representation of the postmodification concepts

Conceptually, a similar strategy may be applied to introduce chiral auxiliary ligands with well-defined binding and catalytic centers to MOPMs that have pendant reactive centers or open metal coordination sites (Fig. 9). Though no CMOPM has been synthesized by this strategy until now, it certainly appears to be quite a feasible and promising strategy.

In Sect. 3, we describe the applications of recently developed, important CMOPMs in chiral separation and heterogeneous asymmetric catalysis with brief structural descriptions.

3 Applications of CMOPMs in Chiral Separation and Catalysis

3.1 Background

For the last few decades, the use of optically pure compounds has significantly increased for economic, environmental, and social reasons. Particularly, pharmaceutical industries desire to produce the active isomer of chiral drugs in optically

pure form to avoid side effects. Among the various methods available to produce selectively single enantiomers, homogeneous chiral catalysis is effective in terms of efficiency and enantioselectivity. However, despite the huge efforts devoted to this field, only few processes (including hydrogenation, epoxidation and reduction) have been applied on an industrial scale [62,63]. One of the main reasons for this unexpected consequence is the difficulty associated with recovery and reuse of highly expensive chiral catalysts. One way to overcome this difficulty is the heterogenization of asymmetric catalysts, which allows facile recovery and reuse of the catalysts [64]. Conventional heterogeneous catalysts are prepared by immobilization of chiral catalysts onto a solid support by covalent bonding or other physical interactions. Mesoporous silica is one of the best choices as solid support for immobilization due to the presence of large well-defined pores with silanol functionality. Organic polymers, ion exchange resins, modified zeolites, and some other materials are also used for immobilization of homogeneous catalysts. This subject has produced several hundred publications and numerous reviews [65–67] to date. In a different immobilization approach, self-supported nonporous coordination polymers with ill-defined structures, but useful for enantioselective catalysis have been prepared by reactions between multitopic chiral ligands and metal ions [68].

All conventional immobilization techniques in chirotechnology suffer from some severe shortcomings. For example, most conventional immobilization methods result in the chiral ligands or catalytically active units randomly anchored onto the solid supports, which often make some of the catalytic sites inaccessible to the substrates. Consequently, the immobilized catalysts display reduced enantioselectivity and lower efficiency in catalysis in comparison with their homogeneous counterparts. As a typical example, the immobilized salen-Mn system of Pini et al. shows only up to 58% ee in epoxydation, which is much lower than that for Jacobsen–Katsuki salen complexes [66,69]. Another major problem is that the bonds between metals and ligands, even if covalent, are often broken under the harsh catalytic reaction conditions and the catalyst breaks away from the solid support and dissolves. This “leaching” process inevitably leads to loss of activity of the catalyst when it is recovered and recycled. Therefore, developing new strategies for the synthesis of more robust metal-ligand conjugates that can sustain harsh conditions is highly desirable.

Chiral separation or sorption is another important technique in chirotechnology. In fact, due to the high cost of chiral catalysts, industries generally prefer chiral separation over asymmetric catalysis to obtain optically pure compounds. As in asymmetric heterogeneous catalysis, a chiral selector (a chiral molecule in optically pure form) can be immobilized on a solid support to make a chiral stationary phase (CSP) of use in direct chiral separation. The basic principle of chiral separation is that the chiral selector interacts differently with the enantiomers of a racemic or enantioenriched mixture to form transient diastereoisomeric species of different stability, and this fine distinction leads to the separation of enantiomers during elution. This topic has also produced a huge number of papers and the readers are referred to the previous reviews for more knowledge on this field [70–73].

3.1.1 Advantages of CMOPMs over Conventional Immobilized Catalysts

In principle, homochiral MOPMs have several advantages over conventional immobilized catalysts: (a) well-ordered structure; (b) high degree of porosity; (c) high density of active catalyst centers; (d) no additional support required. These materials are insoluble in common solvents to fulfill the main prerequisite of a heterogeneous catalyst. Moreover, metals and ligands are strongly bound within the framework to protect "leaching" of the catalyst to the solution and at the same time ensure reusability.

A well-organized chiral pore, large enough for a particular guest molecule to access can induce sufficient enantioselection. The chiral bridging ligands of CMOPMs can provide a chiral environment inside the well-organized cavities/pores, which in principle functions as a chiral selector; therefore, they can be considered to possess a built-in chiral selector. Thus in an ideal situation, CMOPMs also have all the qualities to be efficient CSPs for chiral separation processes.

3.2 Homochiral MOPMs for Enantioselective Separation

Kim and coworkers demonstrated, for the first time, chiral separation in a well-defined microporous cavity utilizing the pores of POST-1 (**4**) (synthesis in Sect. 2.1.2.1) [41]. In POST-1, the carboxylate group of L_5 binds to zinc ions to form an oxo-bridged trinuclear zinc cluster (SBU), which is in turn interconnected via the pyridyl group of L_5 to generate 2D infinite layers consisting of large edge-sharing chair-shaped hexagons with the trinuclear SBU unit at each corner. The chiral 1D channels along the *c* axis have an equilateral triangle-shaped cross section with a side length of ~13.4 Å (Fig. 10). Interestingly, half of six pyridyl groups present in each trinuclear

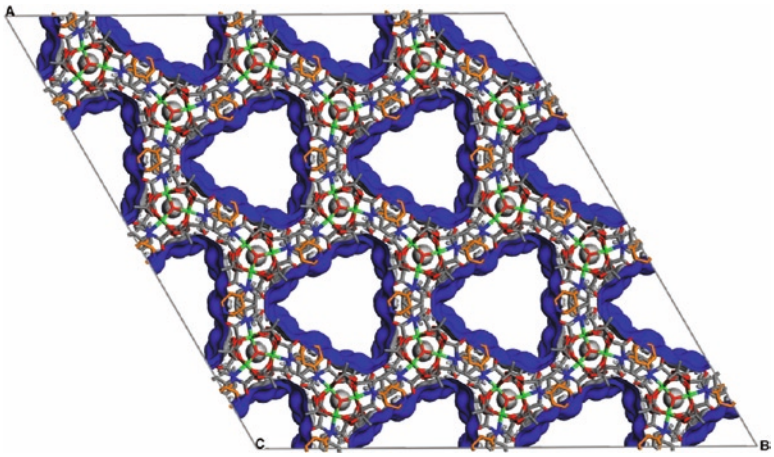

Fig. 10 The Connolly surface of POST-1 showing large chiral channels along the *c* axis. Zn ions (*green*), oxo moieties (*red*) and the pyridyl groups (*orange*) exposed in the channels

unit ($[Zn_3(\mu^3\text{-}O)(L_4\text{–}H)_6]^{2-}$) are coordinated to the zinc ions of three neighboring trinuclear units and the remaining half extrude into the channel without any interactions with the framework, two of which remain protonated.

The presence of large accessible chiral channels in POST-1 (~47%) creates unique opportunity for enantioselective inclusion of chiral molecules. In particular, the large chiral channels of POST-1 were exploited in the separation of racemic $[Ru(bpy)_3]Cl_2$. When L-POST-1 was suspended in a methanolic solution of racemic $[Ru(bpy)_3]Cl_2$, 80% of the exchangeable protons from the dangling pyridine groups were enantioselectively exchanged by $[Ru(bpy)_3]^{2+}$ with 66% enantiomeric excess in favor of the *Δ*-form, which is supported by NMR, UV and CD spectroscopy.

Subsequently, several research groups including Lin, Rosseinsky, Xiong, Fedin and others have designed and synthesized several homochiral porous metal-organic materials capable of enantioselective sorption of chiral organic molecules, which are listed in Table 1.

Xiong and coworkers used an off-the-shelf antimalarial alkaloid, quinine derived enantiopure building block, HQA (6-methoxyl-(8*S*,9*R*)-cinchonan-9-ol-3-carboxylic acid, L_7), to synthesize a homochiral MOPM, $[Cd(QA)_2]$ (**7**, Scheme 1) with an open channel 3D structure, which crystallizes in a distorted octahedral geometry with two

Table 1 List of CMOPMs used for chiral separation

Entry	CMOPMs	Type of Substrate (racemic)	Max. ee (%) achieved	Ref. no.
1	POST-1(**4**)	$[Ru(bpy)_3]Cl_2$	66	[41]
2	$[Cd(QA)_2]$ (**7**)	Small alcohols	98.2	[74]
3	$[Cu_5Cl_6(VB\text{-}N\text{-}ClN)_2]$ (**8**)	2-Butanol	25	[75]
4	$[Cu(PPh_3)(N,N'\text{-}(2\text{-pyridyl-}(4\text{-pyridyl methyl})\text{-amine}))_{1.5}][ClO_4]$ (**9**)	2-Butanol	100	[76]
5	$[Ni_3(btc)_2(3\text{-pic})_6(1,2\text{-pd})_3]$ (**10′**)	Binaphthol	8.3	[77]
6	$[Ni_2(L\text{-asp})_2(bipy)]\cdot CH_3OH\cdot H_2O$ (**11**)	Different diols	53.77	[57]
7	$[Zn_2(bdc)(L\text{-lac})(dmf)]$ (**6**)	Various sulfoxides	60	[56]
8	$[Sm(L_{17e}\text{-}H_2)(L_{17e}\text{-}H_3)(H_2O)_4]\cdot 12H_2O$ (**17e**)	*trans*-1,2-diamino-cyclohexane	13.6	[82]

Ligands: HQA = 6-methoxyl-(8*S*,9*R*)-cinchonan-9-ol-3-carboxylic acid; VB-N-ClN = 4-Vinylbenzyl-cinchonidinium chloride; $L_{17e}\text{–}H_4$ = 2,2′-diethoxy-1,1′-binaphthalene-6,6′-bisphosphonic acid

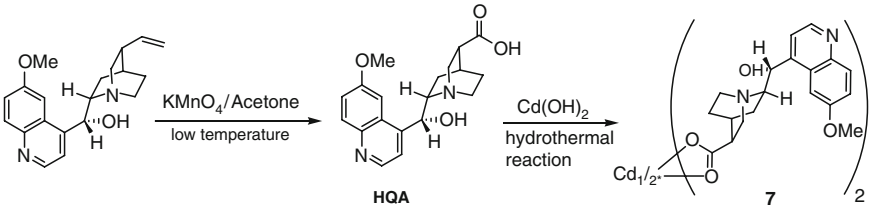

Scheme 1 Synthesis of quitenine (HQA) and the cadmium complex **7**

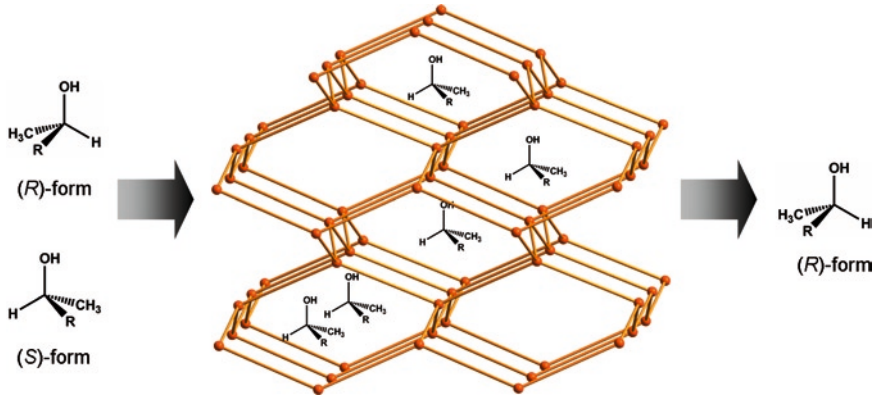

Fig. 11 The diamond-like 3D network of **7**; selective sorption in favor of *S*-alcohol

distinct QA^- ligands bridging the Cd^{2+} ion in different binding modes [74]. From a topological point of view, each Cd^{2+} ion connects with others in a diamond-like fashion, with slight distortion, to form the 3D network (Fig. 11). TGA analysis indicates the robustness of the framework. The adamantane-type cavity within the structure can enantioselectively absorb small organic molecules, such as 2-butanol or 2-methyl-1-butanol. When racemic 2-butanol was mixed with a powdered sample of $[Cd(QA)_2]$ (**7**) under solvothermal conditions, a crystalline sample of (*S*)-2-butanol-$[Cd(QA)_2]$ (**7a**) was obtained. Optical rotation of the desorbed 2-butanol from **7a** matched the standard value of pure (*S*)-2-butanol; the ee value was estimated to be approximately 98.2%. TGA of **7a** shows 8.3% weight loss at 160–204°C corresponding to complete removal of (*S*)-2-butanol, which supports the ability of **7** to include a molecular guest reversibly without changing the framework structure. Relatively larger organic guest, racemic 2-methyl-1-butanol, also gets absorbed in $[Cd(QA)_2]$ (**7b**), but only with 8.4% selectivity in favor of *S*-isomer. Although the homochiral MOPM with a widely used chiral selector in the cavity showed the ability of reversible inclusion of small organic guest molecules, the enantioselectivity drastically decreased with increasing size of the guests. The same group synthesized another 2D homochiral Cu–olefin MOPM (**8**) from a quinine derived ligand, L_8, but its enantioselective sorption ability was rather poor (Table 1) [75].

Xiong et al. also demonstrated that the chiral 2D framework $[Cu(PPh_3)(N,N'$-(2-pyridyl-(4-pyridyl methyl)-amine))$_{1.5}]\cdot ClO_4$ (**9**), with triangular cavities, synthesized from achiral components, $[Cu(MeCN)_2(PPh_3)_2][ClO_4]$ and *N*,*N*′-(2-pyridyl-(4-pyridyl methyl)-amine) can enantioselectively include 2-butanol [76]. Spontaneous resolution produced crystalline inclusion compound **9**·1.5(2-butanol), which was structurally characterized. They manually separated the enantiomorphic forms of **9**·1.5(2-butanol) according to their CD spectra in solid state and evacuated at 100°C to collect enantiopure 2-butanol. Although this work provides an economical route to enantioselective separation of racemic small diols, the separation

process is rather time consuming. The route is also not general, as the framework does not guarantee inclusion of other kind of molecules.

The (10,3)-a net based chiral frameworks developed by Rossenesky et al., showed enantioselective sorption properties [77]. The doubly interpenetrating, distorted (10,3)-a framework, **1**, showed a tendency to collapse upon removal of the guests from its cavity and the resulting nonporous amorphous phase (**1′**) adopted a new 6,3-layered structure upon reexposure to pyridine. Interestingly, the desolvated amorphous phase **1′** can regenerate its original 2 X (10,3)-a network structure upon exposure to 3-picoline, which is found to be stable even after the loss of guest molecules. They separately synthesized the 3-picoline ligated framework, **10**, having a molecular formula $[Ni_3(btc)_2(3\text{-pic})_6(1,2\text{-pd})_3]\cdot 9(1,2\text{-pd})_9\cdot 11(H_2O)$ from enantiopure 1,2-pd. In contrast to **1**, after guest removal at 150°C, **10** retains crystallinity with identical space group symmetry and slightly modified unit cell parameters. Despite the same framework structure, their striking difference in stability is due to unconventional H-bonding between the methyl C–H of the picoline moiety and the noncoordinating oxygen of the btc carboxylate (Fig. 12a).

The estimated 47% void for the desolvated phase **10′** is in good agreement with the Dubinin-Radushkevich micropore volume (0.63(1) mL g^{-1}). In **10′**, two large pores with different diameters (12 Å and 13.6 Å) are available for guest sorption (Fig. 12b). However, the apparent advantage of a larger window goes against enantioselective sorption of small chiral molecules. Although relatively large binaphthol (9 × 9 Å) is enantioselectively sorbed by (*S*)-**10′** (but with only 8.3% ee), smaller guests such as ethyl 3-hydroxybutyrate and fenchone show ready sorption but no enantioselectivity. Thus, a close match of the dimensions of chiral channels and the size of the chiral guests is required for the microporous substances like **10′** to discriminate between the enantiomers. This work requires further investigation of the binding behavior of guest molecules with the chiral pockets of hosts to rationally design and synthesize materials with high enantioselective sorption ability.

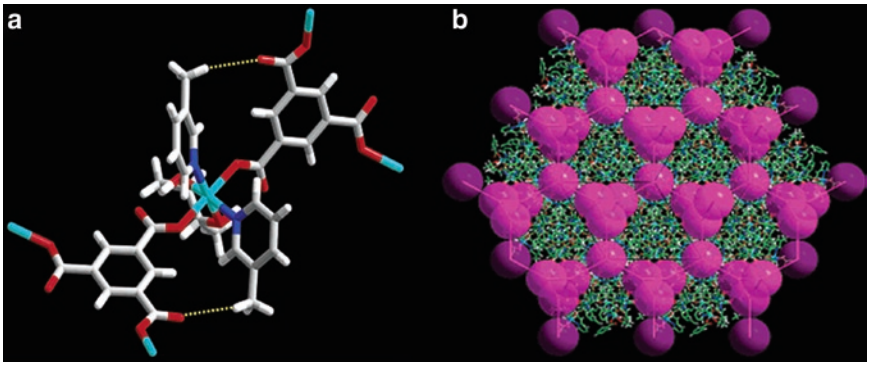

Fig. 12 (**a**) C–H···O interaction (*yellow dotted line*) between the methyl group of the 3-picoline and the nonbonding carboxylate oxygen atom (*red*) of the btc framework forming node in **10**; Ni centers (*light blue*). (**b**) the cavities and interconnecting channels (*purple*) that constitute the chiral porosity of the material. In panels (**c**) and (**d**), the structure is viewed along the 111 direction

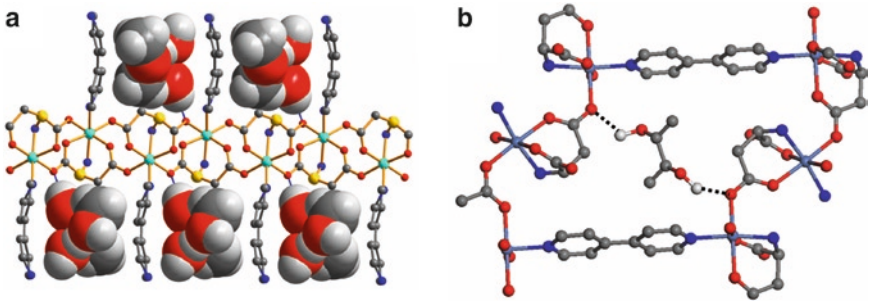

Fig. 13 (**a**) 2D layers of framework **11**; the disordered methanol and water guests that occupy the channels are represented with space filling spheres. (**b**) Location of 1,2-propanediol within the channels of **11**; methyl group is omitted for clarity. Hydrogen bonds are represented by *dashed blue lines*. Ni *cyan*, C *gray*, H *white*, N *blue*, O *red*

Natural amino acids have also been utilized as building blocks to prepare homochiral MOPMs with enantioselective sorption ability [57]. Solvothermal reaction of Ni(L-asp)·3H_2O and 4,4′-bipyridine (bipy) in a water/methanol mixture at 150°C affords the homochiral open-framework material [Ni_2(L-asp)$_2$(bipy)]·CH_3OH·H_2O (**11**). In the crystal structure, an aspartate molecule binds to one nickel center in a tridentate fac mode and two other Ni centers in a monodentate mode to form chiral neutral Ni(L-asp) layers (Fig. 13a). These Ni(L-asp) layers are bridged by bipy ligands to form a pillared structure with 1D channels with a small cross section of 3.8×4.7 Å. The framework is robust and permanently porous as revealed by PXRD and CO_2 measurements, and the estimated guest-accessible volume of the framework is 23.1%. The enantioselective sorption property of **11** examined with different positional isomers of diols starting from propanediol to hexanediol shows ee values up to 53.7%. The host derived from D-aspartate also shows the same degree of enantioenrichment but for the opposite enantiomer in all cases. Several diols of a fixed chain length reveal a large difference in enantioselection. For example, the four carbon chain diols, 1,2-butanediol and 2,3-butanediol show considerably reduced enantioselection (5.0 and 1.5% ee, respectively) with respect to 1,3-butanediol (17.9% ee). The 1,3-disposition of diols seems to be favorable and the highest value of ee was observed for 2-methyl-2,4-pentanediol (53.7%). Although the crystals of the host–guest complexes of **11** could not be grown, the interactions of the diol guests with the internal surface of the porous material can be visualized from their model compound [Ni_2(L,D-asp)$_2$(bipy)]·CH_2(OH)CH(OH)CH_3 (**12**). The crystal structure of **12** showed that the guest located in the pocket while bridging two Ni(asp) layers through hydrogen bonding (Fig. 13b). The docking procedure also proved that the interaction of **13** with the two guest molecules of same alkyl-chain lengths, 1,2-pentanediol and 2-methyl-2,4-pentanediol, sit in exactly identical sorption sites in the pocket (defined by two aspartate and two bipy molecules on opposite sides of the channel), but interact differently with the framework. Both alcoholic groups of (*S*)-2-methyl-2,4-pentanediol participate in hydrogen bonding

with the framework **11** and consequently account for its high ee value. While the tertiary alcohol group forms hydrogen bond with the β-carboxylate group of an aspartate residue (OH···O 2.390 Å), the secondary alcohol group forms an H-bond with the amine group of another aspartate residue (O···HN 2.663 Å). In contrast, only the secondary alcohol group of (*S*)-1,2-pentanediol interacts with the framework of **11** by hydrogen bonding with the β-carboxylate group of an aspartate residue (OH···O 2.667 Å) and the amine group of another aspartate residue (O···HN 2.507 Å). These different modes of interaction account for the observed differences in enantioselection. This descriptive study demonstrates that the surface chemistry of channels is an important factor in addition to their size for an improved enantiosorption of guests by chiral MOPMs.

Permanently porous, homochiral framework, $[Zn_2(bdc)(L\text{-lac})(dmf)]\cdot(DMF)$ (**6**·DMF), was utilized in enantioselective sorption of pharmaceutically important sulfoxides [56]. The material **6** forms medium-sized pores (~5 Å) by the attachment of bdc with 1D chain like chiral SBU containing L-lactates and zinc ions (Fig. 14), which has been exploited in enantiosorption of sulfoxides as well as the enantioselective oxidation of thioethers (see below). The DMF molecules in the pores can be removed by heating at 110–200°C; however, prolonged heating causes partial

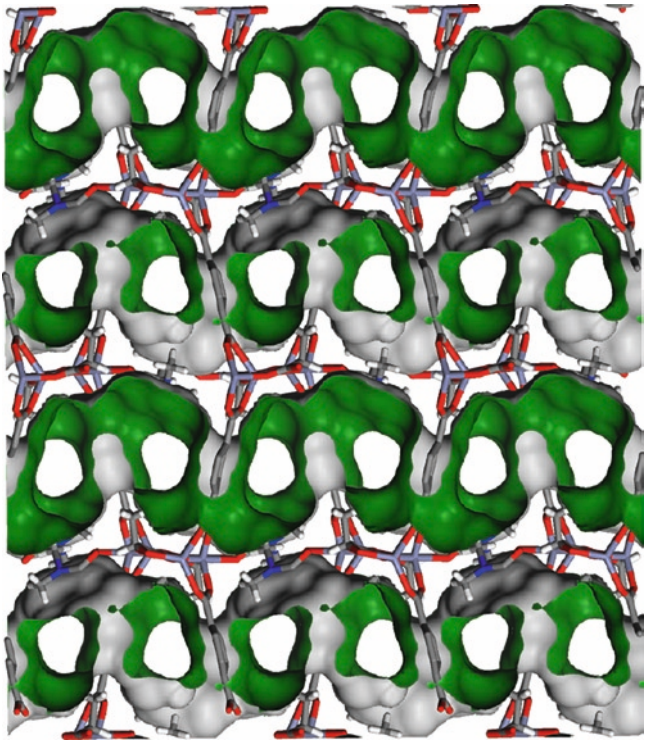

Fig. 14 The Connolly surface of framework **6** showing medium-sized pores (~5 Å) and 1D channels

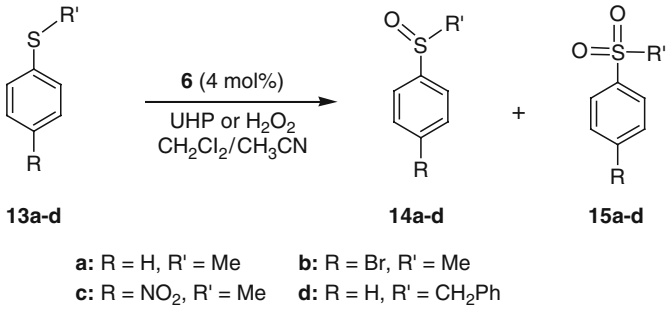

Scheme 2 Oxidation of sulfides catalyzed by **6**

collapse of the framework. The partially evacuated material **6**·$(DMF)_{0.4}$ showed significant sorption ability for the aromatic sulfoxides with small substituents such as **14a** and **14b**: 0.68 and 0.18 molecules, respectively, per formula unit of **6** with moderate ee values (20% for **14a** and 27% for 14b) in favor of *S*-isomer. However, pores of **6** were unable to incorporate larger sulfoxides such as **14c** and **14d**. More interestingly, after extraction of the absorbed molecule, the material **6** can be reused in the next cycle with no appreciable change in its sorption ability.

The material **6** showed a remarkable catalytic activity in the oxidation of thioethers **13** to sulfoxides **14** by urea hydroperoxide (UHP) or H_2O_2 (Scheme 2). Although the conversion and selectivity (for **14** over **15**, >90%) was reasonable with UHP for the substrates with smaller substituents, **13a** and **13b**, the ones with bulkier substrates **13c** and **13d** failed to produce any measurable conversion. The conversion increases to 100% by changing UHP with H_2O_2. The catalytic activity of **6** for selective sulfoxidation remains similar even after 30 cycles. Despite the fact that no asymmetric induction was found in the catalytic sulfoxidations, enantioenriched sulfoxides were obtained by enantioselective sorption of the resulting racemic mixture by the chiral pores of **6**, which occured simultaneously with the catalytic process. Thus, after catalytic oxidation of **13a**, (*S*)-**14a** was preferentially absorbed by the pore of **6** leaving exactly equal amount of the excess *R*-enantiomer in the solution phase (~20% ee). The combination of high catalytic activity and enantioselective sorption property of **6** provides a unique opportunity to device a one-step process to produce enantioenriched products.

Fedin and Bryliakov extended this work to demonstrate the use of **6**·DMF as a CSP for the separation of a racemic mixture of **14a** [78]. The wide difference in the sorption ability between the *S*- and *R*-enantiomers instigates the plan to use **6** as a CSP for liquid column chromatography. Interestingly, both electronic and steric effects of the substituents in the aromatic ring play an important role in determining sorption constant and ee of sorption values. An electron withdrawing substituent at the aromatic ring reduces both sorption constant and ee of sorption by reducing coordination ability of the sorbate (Table 2, entry 1 and 4). Although an electron donating substituent increases the sorption constant value, additional substituent in the aromatic ring results in slower internal diffusion leading to poorer enantioselection (Table 2, entry 3). However,

Table 2 The apparent sorption constants of enantiomerically pure sulfoxides on 6

Entry	Sulfoxide	K_S[a] M^{-1}	K_R[a] M^{-1}	α[b]	ee %[c] (sorption)
1	*p*-BrPhSOMe	11	10	1.1	7 (0.15)
2	PhSOMe	68	15	4.5	60 (0.30)
3	*p*-MePhSOMe	326	129	2.5	38 (0.53)
4	*p*-NO_2PhSOMe	n.m.	n.m.	–	~0 (0.13)
5	PhSOi-Pr	54	12	4.5	55 (0.20)

[a] K_S = sorption constant for *S*-isomer, K_R = sorption constant for *R*-isomer
[b] Stereoselectivity factor, $\alpha = K_S/K_R$
[c] The highest measured ee of the sorbate, and the respective sorption values, in the molecules per formula unit [Zn_2(bdc)(L-lac)(dmf)]

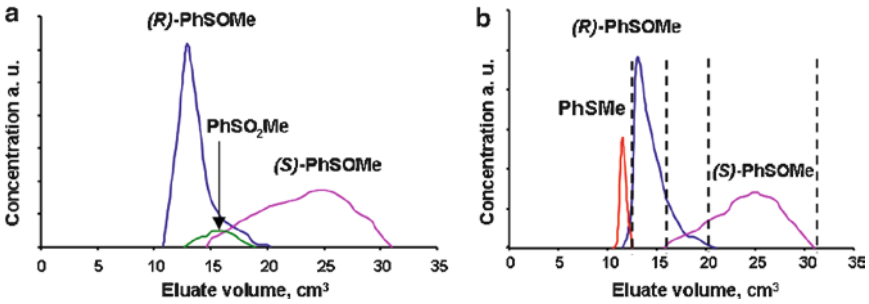

Fig. 15 Catalytic oxidation of PhSMe/enantiomeric separation of PhSOMe over a column with **6**·DMF, using 5-fold (**a**) and 1.5-fold (**b**) excess of the oxidant. Elution rate: 2 $cm^3 h^{-1}$; eluent CH_2Cl_2/CH_3CN:: 85:15

steric crowding at the sulfur atom does not alter the selectivity factor (entry 5), whereas, methyl phenyl sulfoxide (entry 2) with an unsubstituted aromatic ring fits best in the pores of **6**, thus giving best separation of enantiomers.

By taking advantage of both catalytic activity and enantioselective sorption ability of **6** discussed above, a one-step reaction-purification system was developed to synthesize optically pure sulfoxides. In an illustrative example, PhSMe was chosen as a substrate. A mixture of the sulfide and H_2O_2 in 0.01 M of DMF in CH_2Cl_2/CH_3CN was loaded on top of the column packed with **6** and eluted with the same solvent mixture. The *R*-isomer of the corresponding sulfoxide was eluted first as it has low affinity with **6**, followed by *S*-isomer (Fig. 15). Excess amount of H_2O_2 (5-fold) forms about 5% of sulfone (the over-oxidation product), but a little excess (1.5-fold) of the oxidant, even though left out some disulfide in the mixture (conversion = 91%), affords pure enantiomers ca. 35% each based on the starting PhSMe to offer a overall isolated yield of 70% (Fig. 15b). This was the first demonstration of an application of CMOPMs in chiral chromatography. Furthermore, the tandem

procedure to produce optically pure product is attractive in terms of production cost and time consumption, and tempts further studies in this direction.

There are a couple of reports from Pal and coworkers on chiral MOFs capable of enantiospecific inclusion of chiral rotamers [79,80]. Although this type of work is worthwhile from a theoretical point of view, in practical sense the desorbed rotamer will racemize immediately through rotation around the C–C bond, making isolation of optically pure rotamers impossible.

Certainly, a couple of important points can be made from the entire collection of work on chiral separation by CMOPMs: (a) the size of the pore should fit the substrate for proper enantiodifferenciating interactions; (b) different mode of interactions of similar kind of substrates with the surface of the pores/channels alters enantioselection ability. So far, the chiral separation ability of chiral metal-organic assemblies has been studied mostly with small molecules. However, the main goal of designing these materials is to utilize them for the separation of the enantiomers of relatively large molecules (e.g., drugs) and further studies are required in this direction.

3.3 Homochiral MOPMs as Heterogeneous Catalysts

Proper incorporation of suitable catalytic units into CMOPMs with accessible pores for organic substrates can generate potentially useful solid matrices for asymmetric transformations. Fujita et al. first explored the utility of a hybrid organic–inorganic solid as a heterogeneous Lewis acid catalyst [40]. Later, Aoyama and coworkers also demonstrated the catalytic properties of MOPMs for Diels–Alder reactions [81]. In both the cases, however, achiral metal-organic assemblies were used. Despite the huge potential, the use of homochiral metal-organic assemblies for the applications in asymmetric catalysis was not reported until 2000 when Kim and coworkers reported the first asymmetric induction catalyzed by a homochiral MOPM [41]. After this, a number of chiral MOPMs have been synthesized and their heterogeneous, enantioselective catalytic activities studied (Table 3).

The key structural feature of POST-1 - the presence of dangling pyridine groups in the channels - affords a unique opportunity to perform asymmetric heterogeneous catalysis. Thus, potentially, any base catalyzed reactions (e.g., esterification or hydrolysis) can be performed with POST-1. Moreover, chiral pores should induce a degree of enantioselectivity in the final product mixture. The catalytic activity of POST-1 in the transesterification reaction was examined. Although the reaction of **16** and ethanol in the presence of POST-1 in carbon tetrachloride produced ethyl acetate in 77% yield, little or no transesterification occured without POST-1 or with the *N*-methylated POST-1 (Sect. 2.2). The post chemical modification of the pyridine groups in POST-1 proves the role of free pyridine moiety in transesterification reaction. Transesterification of ester **16** with bulkier alcohols such as isobutanol, neopentanol, and 3,3,3-triphenyl-1-propanol occurs at a much slower rate under otherwise identical reaction conditions. Such size selectivity suggests that catalysis mainly occurs in the channels.

Table 3 List of CMOPMs used in heterogeneous asymmetric catalysis

Entry	CMOPMs	Type of reaction[a]	Catalyst loading (mol %)	Yield (%)	ee (%)	Reference number
1	POST-1 (**4**)	Transesterification	10	77	~8	[41]
2	$[Sm(L_{17e}–H_2)(L_{17e}–H_3)(H_2O)_4]\cdot 12H_2O$ (**17e**)	Cyanohdrine formation	10	55–69	<5	[82]
		Ring opening of *meso*-anhydride	10	81	<5	
3	$Zr[Ru(L_{18}$ or $L_{19})(dmf)_2Cl_2]\cdot 2MeOH$ (**18**, **19**)	Hydrogenation of β-keto esters	0.1–1	70–100	65–95	[83]
4	$Zr[Ru(L_{19}–H_4)(DPEN)Cl_2]\cdot 4H_2O$ (**20**) and sameskeleton with L_{18} (**21**)	Hydrogenation of aromatic ketones	0.005–0.1	>99	80–99	[84]
5	$ZrL_{22–24}$ (**22–24**) (active catalyst = (**22–24**)·Ti)	Diethylzinc additions to aromatic aldehydes	20–50	70–99	30–72	[85]
6	$[Cd_3Cl_6(L_{25})_3]\cdot 4DMF\cdot 6MeOH\cdot 3H_2O$ (**25**) (active catalyst = **25**·Ti)	Diethylzinc additions to aromatic aldehydes	13	>99	80–93	[86]
7	$[Cd_3(L_{25})_4(NO_3)_6]\cdot 7MeOH\cdot 5H_2O$, (**26**)(active catalyst = **26**·Ti)	Diethylzinc additions to aromatic aldehydes	12–25	>99	45–90	[87]
8	$[Zn_2(bpdc)_2L_{28}]\cdot 10DMF\cdot 8H_2O$ (**28**)	Epoxidation	0.025	71	82	[54]
9	$[Cu_2(L_{29})_2(H_2O)_2]\cdot MeOH\cdot 2H_2O$ (**29**)	Ring opening of epoxide	5	1–54	0–51	[88]
10	$[Zn_2(bdc)(L\text{-}lac)(dmf)]$ (**6**)	Oxidation of sulfoxides	2	60–100	0[b]	[56]
11	$[Cu_2(D\text{-}/L\text{-}asp)_2bpe]\cdot$(guests)	Methanolysis of *trans*-2,3-epoxybutane	10	30–65[c]	3–17[c]	[89]

[a] Each CMOPM is used as asymmetric catalyst for one (or more) type of reaction on a series of substrates; the range of catalyst loading, yields and ee values are given in the subsequent columns

[b] Although no asymmetric induction was observed, the products enantioselectively absorbed inside the pores with ee ranging from 20 to 27% depending on substrates leaving equal amount of other enantiomer in the solution

[c] Depending on reaction condition both yield and ee vary for a single substrate

Ligands: $L_{17}–H_4$ = 2,2′-diethoxy-1,1′-binaphthalene-6,6′-bisphosphonic acid; $L_{18}–H_4$ = 2,2′-bis(diphenylphosphino)-1,1′-binaphthyl-6,6′-bis(phosphonic acid); $L_{19}–H_4$ = 2,2′-bis(diphenylphosphino)-1,1′-binaphthyl-4,4′-bis(phosphonic acid); $L_{22}–H_4$ = 2,2′-dihydroxy-1,1′-binaphthyl-6,6′-bis(phosphonic acid); $L_{23}–H_4$ = 2,2′-dihydroxy-1,1′-binaphthyl-6,6′-bis(vinylphos-phonic acid); $L_{24}–H_4$ = 2,2′-dihydroxy-1,1′-binaphthyl-6,6′-bis(styrylphosphonic acid); L_{25} = (*R*)-6,6′-dichloro-2,2′-dihydroxy-1,1′-binaphthyl-4,4′-bipyridine; L_{28} = (salen)$Mn^{III}Cl$ (salen = [(*R*,*R*)-(–)-1,2-cyclohexanediamino-*N*,*N*′-bis(3-*tert*-butyl-5-(4-pyridyl)-salicylidene)]); H_2bpdc = biphenyldicarboxylic acid; L_{29} (H_2BDA) = (*R*)-5,5′-(2,20-dihydroxy-1,10-binaphthalene-5,5′-dicarboxylic acid; bpe = 1,2-bis(4-pyridyl)ethylene

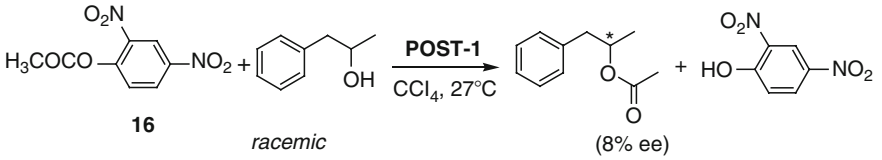

Scheme 3 Catalytic activity of POST-1 in transesterification

Most interestingly, POST-1 showed enantioselective catalytic activity for transesterification of **16**. The reaction of **16** with a large excess of *rac*-1-phenyl-2-propanol in the presence of D-POST-1 or the enantiomorphic L-POST-1 produces corresponding esters with ~8% enantiomeric excess in favor of *S*- or *R*-enantiomer, respectively (Scheme 3). The low enantioselectivity may be the consequence of the fact that the catalytically active units (dangling pyridyl groups) are a bit too far away from the chiral wall of the pores. Even though the ee value is modest, this is the first observation of an asymmetric induction in the catalytic reactions mediated by modular porous materials. This seminal work triggered interest among others to rationally design chiral ligands and synthesize corresponding homochiral metal-organic systems for various heterogeneous catalysis reactions. Later, Gao et al. further explored the utility of POST-1 in supramolecular photochirogenesis [82].

Lin and coworkers adopted a systematic approach toward designing homochiral MOPMs using BINAP units as a building block for chiral separation and asymmetric heterogeneous catalysis [83–88]. They first prepared a series of homochiral porous lamellar lanthanide bisphosphonates of general formula $[Ln(L_{17}–H_2)(L_{17}–H_3)(H_2O)_4]\cdot xH_2O$ ($L_{17}–H_4$ = 2,2′-diethoxy-1,1′-binaphth-alene-6,6′-bisphosphonic acid, Ln = La, Ce, Pr, Nd, Sm, Gd, Tb, x = 9–14, **17a–g**) (Scheme 4) and explored their applications in heterogeneous catalysis and chiral separations [83]. The CMOPMs adopt 2D layered structures with square antiprismatic Ln center that have four H_2O molecules and four oxygen atoms of the phosphonate groups of four different binaphthylbisphosphonates in the coordination sphere (Fig. 16). The space filling model suggested that **17a–g** contain large chiral channels with largest dimension of 12 Å. PXRD pattern of desolvated **17a–g** which

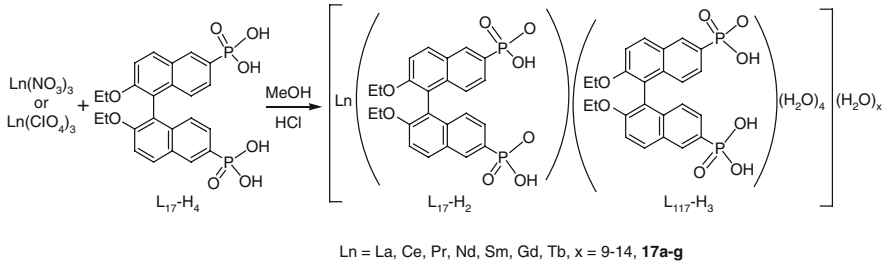

Scheme 4 Preparation of $[Ln(L_{17}–H_2)(L_{17}–H_3)(H_2O)_4]\cdot 12H_2O$ compounds

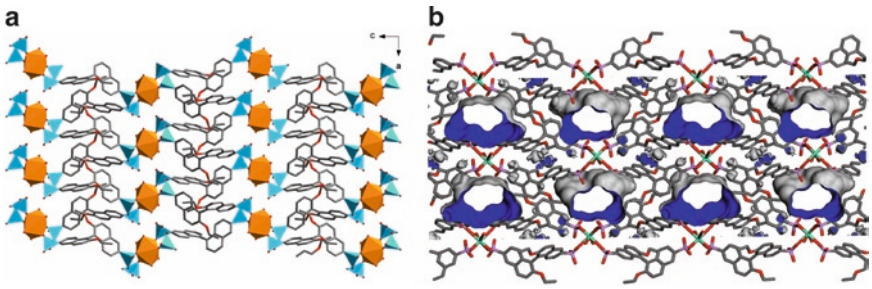

Fig. 16 (**a**) A view of 2D framework of **17f** down the *b* axis; the coordination environments of P atoms and Gd atoms are represented with *blue* and *orange* polyhedra, respectively. (**b**) The Connolly surface of framework **17f** showing 1D channel between 2D layers

suggests that the local coordination environment is retained during desolvation. They exhibit reversible dehydration and framework stability. Compound **17e** was utilized as a chiral Lewis acid catalyst for several organic transformations, including cyanosilylation of aldehydes, ring opening of mesocarboxylic anhydride, and Diels–Alder reactions with high yields but disappointingly low ee (<5%). Such a lack of enantioselectivity was a direct consequence of the highly symmetrical coordination environment around the catalytically active Sm centers and points out the limitations of such simple M-L-M systems.

To improve the enantioselectivity, Lin et al. designed chiral bridging ligands with duel functional groups. While primary functional groups form an extended network structure, chiral secondary functionalities can be used to decorate the porous metal-organic structure and subsequently generate asymmetric catalytic sites, which are accessible to the organic substrates via the open channels or cavities. This strategy was utilized to synthesize porous zirconium phosphonates with pendant chiral chelating bisphosphanes groups [84]. Two new chiral porous Zr-phosphonates with approximate formulae $Zr[Ru(L_{18})(dmf)_2Cl_2]\cdot 2MeOH$ (Zr–Ru–L_{18}, **18**) and $Zr[Ru(L_{19})(dmf)_2Cl_2]\cdot 2MeOH$ (Zr–Ru–L_{19}, **19**) were synthesized by a sequence of reactions starting from BINAP derivatives 2,2′-bis(diphenylphosphino)-1,1′-binaphthyl-6,6′-bis(phosphonic acid) (L_{18}–H_4) and 2,2′-bis(diphenylphosphino)-1,1′-binaphthyl-4,4′-bis(phosphonic acid) (L_{19}–H_4), respectively (Scheme 5). N_2 adsorption measurements indicated that Zr–Ru–L_{18} and Zr–Ru–L_{19} possess high degree of porosity, while powder XRD indicated that both solids are amorphous. Both solids have proved very effective as heterogeneous catalysts for asymmetric hydrogenation of keto esters. Zr–Ru–L_{18} showed better catalytic activity than the other compound for the hydrogenation of a wide range of β-alkyl-substituted β-keto esters with complete conversions and ee values ranging from 91.7 to 95.0% (Table 4). The enantioenrichment of Zr–Ru–L_{18} is the same as the parent homogeneous BINAP–Ru catalyst. The system shows less than 0.01% leaching during the catalytic reactions. The same catalytic activity of Zr–Ru–L_{18} can be retained up to five cycles of hydrogenation with no significant deterioration of enantioselectivity.

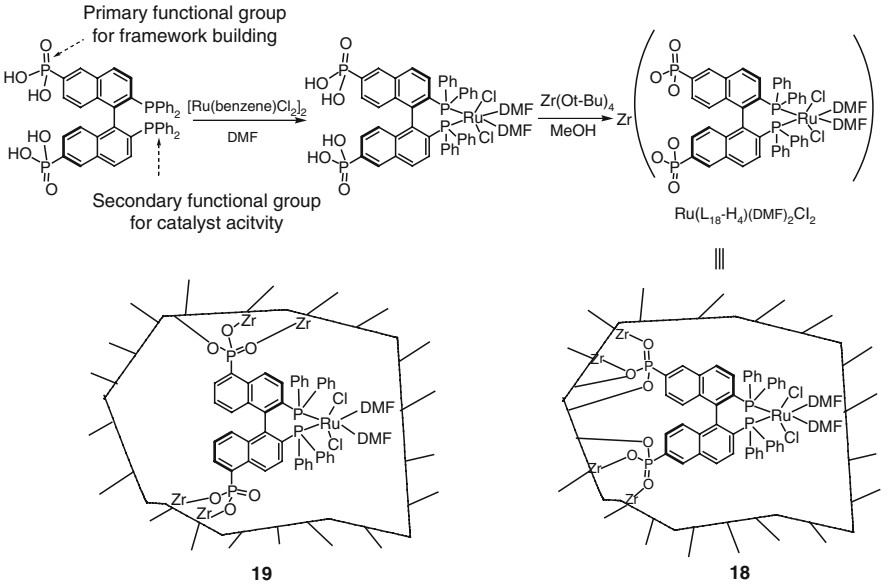

Scheme 5 Synthesis of Zr–Ru–L_{18} and Zr–Ru–L_{19}

Table 4 Heterogeneous asymmetric hydrogenation of β-keto esters with **18** and **19**

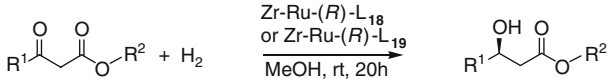

Substrate	Catalyst loading [%]	T (°C)	H_2 Pressure [psi]	Zr-Ru-L_{18} ee (% yield)	Zr-Ru-L_{19} ee (% yield)
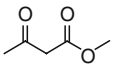	1	60	700	94.0 (100)	73.1 (90)
	1	RT	1400	95.0 (100)	
	0.1	60	700	93.3 (100)	
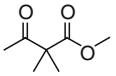	1	RT	1400	93.3 (100)	78.8 (70)
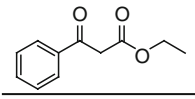	1	RT	1400	69.6 (100)	15.7 (50)

Incorporation of DPEN (1,2-diphenylethylenediamine) in the same skeleton of Zr-phosphonates improves both catalytic activity and enantioselectivity to almost quantitative value [85]. The syntheses involved the same sequence of reactions as in the previous work and TGA and microanalysis suggested their formulae as

Table 5 Heterogeneous asymmetric hydrogenation of aromatic ketones with **20** and **21**

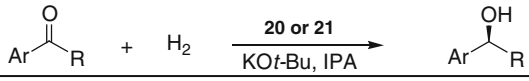

Substrate	Catalyst loading [%]	KO^{t}Bu	**20** ee	**21** ee
Ar: Ph, R: Me	0.1	1	96.3	79.0
Ar: 4?-*t*-Bu-Ph, R: Me	0.1	1	99.2	91.5
Ar: 1-naphthyl, R: Me	0.1	1	99.2	95.8
	0.02	0.4	98.9	
	0.005	0.02	98.8[a]	
	0.005	0.02	98.6[b]	

[a]70% conversion;
[b]40h reaction time

$Zr[Ru(L_{19}–H_4)(DPEN)Cl_2]·4H_2O$ (**20**) and $Zr[Ru(L_{18}–H_4)(DPEN)Cl_2]·4H_2O$ (**21**), respectively. N_2 adsorption measurements indicated that both **20** and **21** are highly porous with rather wide pore size distributions. The enantioselective catalytic activity of **20** and **21** for the hydrogenation of aromatic ketones was studied (Table 5). Only 0.1 mol% loading of catalyst **20** in isopropanol was sufficient to hydrogenate acetophenone with complete conversion and 96.3% ee, which is significantly higher than that observed for the parent Ru–BINAP–DPEN homogeneous catalyst (~80% ee) under similar conditions [89,90].

Although **21** also showed catalytic activity for the same reaction, enantioselectivity is rather modest. A series of substrates was tested with **20,** which showed complete conversion with high ee as illustrated in Table 5. Lowering the amount of catalyst (**20**) to 0.02 mol% does not affect the ee, while a catalyst concentration of 0.005% requires a longer time (40 h) for completion but with the same ee conversion. The TOF is calculated to be 500 h^{-1} at complete conversion and 700 h^{-1} at 70% conversion. Compound **20** can be readily recycled and reused up to eight cycles without any loss of enantioselectivity. High activity and enantioselectivity of these solids thus hold the promise for developing better and practically useful heterogeneous asymmetric catalysts with a similar designing approach.

Lin et al. also used BINOL linkers with phosphonate groups at a proper position to form the main framework with zirconium and explored the presence of the free hydroxyl functional groups as a catalyst holding unit to develop Ti-based catalysts for diethyl zinc addition to aromatic aldehydes [86]. Amorphous chiral porous zirconium phosphonates $Zr–L_{22}$ to $Zr–L_{24}$ (**22**–**24**) when treated with excess $Ti(Oi–Pr)_4$, generate active catalysts, which convert several aromatic aldehydes to corresponding chiral secondary alcohols with high conversion but slightly lowered ee values (up to 72%) (Scheme 6). However, the variable linkers between the BINOL moiety and the phosphonate groups do not show much effect on catalytic activity or enantioselection.

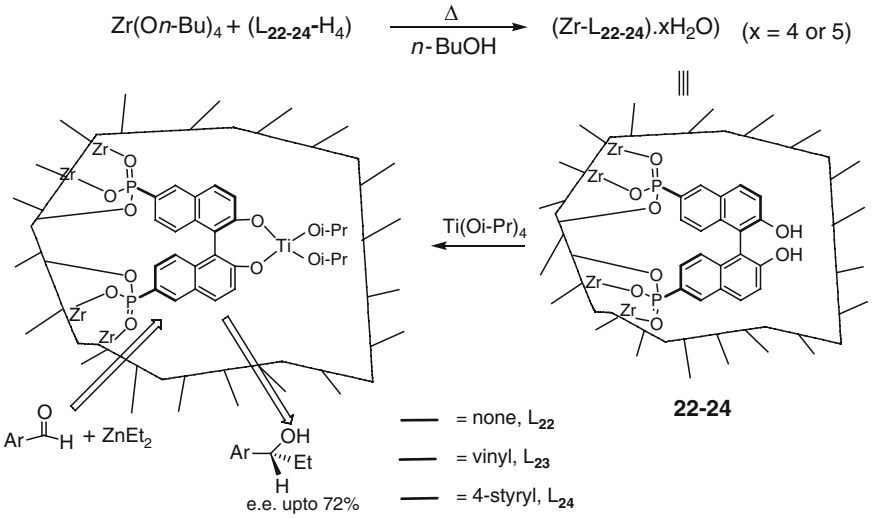

Scheme 6 Synthesis of BINOL derived Ti-based catalysts **22**–**24**

By incorporating a rigid linking arm at the 4 and 4′ positions of BINOL unit, Lin et al. finally succeeded in synthesizing a crystalline homochiral MOPM (**25**) [87]. The BINOL derivative, (*R*)-6,6′-dichloro-2,2′-dihydroxy-1,1′-binaphthyl-4,4′-bipyridine (L_{25}) when reacted with $CdCl_2$, afforded the CMOPM with molecular formula $[Cd_3Cl_6(L_{25})_3]\cdot 4DMF\cdot 6MeOH\cdot 3H_2O$, **25**, which crystallizes in the triclinic P_1 space group. The Cd(II) centers in **25** are doubly bridged by the chlorides to form 1D zigzag $[Cd(\mu^2\text{-}Cl)_2]_n$ chains, which are further connected through the pyridyl groups of L_{25} to form a noninterpenetrating 3D network with large chiral channel with the cross section of 1.6 × 1.8 nm (Fig. 17a). PLATON calculations indicated that **25** contains 54.4% solvent accessible void space. X-ray powder diffraction and CO_2 adsorption measurements of **25** indicated that the porous framework was maintained even after evacuation.

Although two of the three L_{25} ligands in a unit cell are shielded from the open channels, **25** was utilized in asymmetric catalysis by taking advantage of the readily accessible chiral dihydroxy groups of the third ligand (Fig. 17b). Treatment of **25** with excess $Ti(Oi\text{–}Pr)_4$ formed an active catalyst (designated as **25**·Ti) for the diethylzinc addition reactions to a range of aromatic aldehydes with complete conversion and high enantioselectivity (up to 93% ee) (Table 6). The level of enantioselectivity is similar to that of the homogeneous analog under similar conditions (94% ee). Control experiments with a series of larger aldehydes of varying sizes (from 0.8 to 2.0 nm) confirmed that the catalytic activity was dependent on the aldehyde size, and no catalytic activity was observed when the size of the aldehyde became larger than the open channel size. This set of experiments clearly demonstrates that **25**-Ti is a true heterogeneous asymmetric catalyst as both $ZnEt_2$ and

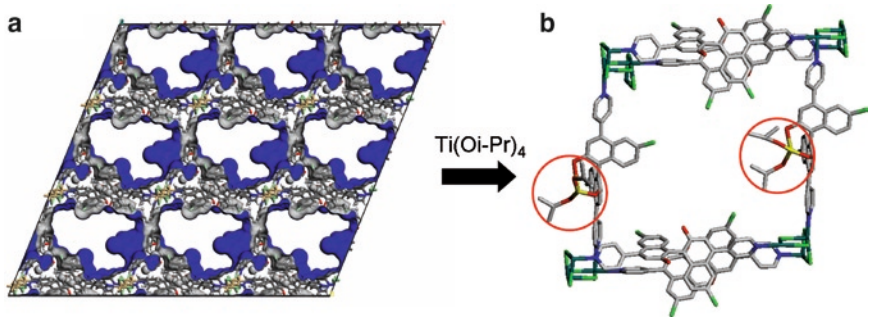

Fig. 17 (**a**) The Connolly surface of **25** clearly showing the large 1D chiral channels; (**b**) Schematic representation of the active (BINOL)Ti(Oi-Pr)$_2$ catalytic sites (marked by *red circle*) in the open channels of **25**

Table 6 Ti(IV)-catalyzed $ZnEt_2$ additions to aromatic aldehydes with (*R*)-**25**

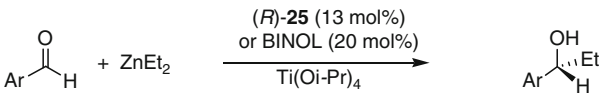

	BINOL		(*R*)-**25**·Ti	
Ar	Conv (%)	ee (%)	Conv (%)	ee (%)
1-Naph	>99	94	>99	93
Ph	>99	88	>99	83
4-Cl-Ph	>99	86	>99	80

All the reactions were conducted at room temperature in presence of excess Ti(Oi-Pr)

aromatic aldehyde accessing the catalytic sites via the open channels generate chiral secondary alcohols.

Very recently, Lin et al. examined the relationship between the framework structure and the catalytic activity of homochiral MOPMs [88]. The same ligand L_{25} was utilized to synthesize two more crystalline chiral MOPMs $[Cd_3(L_{25})_4(NO_3)_6]\cdot 7MeOH\cdot 5H_2O$, **26**, and $[CdL_{25}(H_2O)_2][ClO_4]_2\cdot DMF\cdot 4MeOH\cdot 3H_2O$, **27**. Compound **26** crystallizes in the tetragonal $P4_122$ space group with 1.5 Cd(II) centers in the asymmetric unit. Two independent L_{25} are linked to two different Cd(II) atoms to form 2D square grids and 1D zigzag polymeric chains, respectively. These are further joined to each other by the bridging nitrate groups to form a twofold, interpenetrated, 3D framework with large interconnected channels of 4.9 × 13.1 Å parallel to the a and b axes and 13.5 × 13.5 Å parallel to *c* axis (Fig. 18a); whereas, compound **27** crystallizes in $P4_32_12$ space group, and forms an interlocked 2D rhombic grid and possesses 1D channels ~1.2 × 1.5 nm in dimension (Fig. 18b). PXRD spectrum of

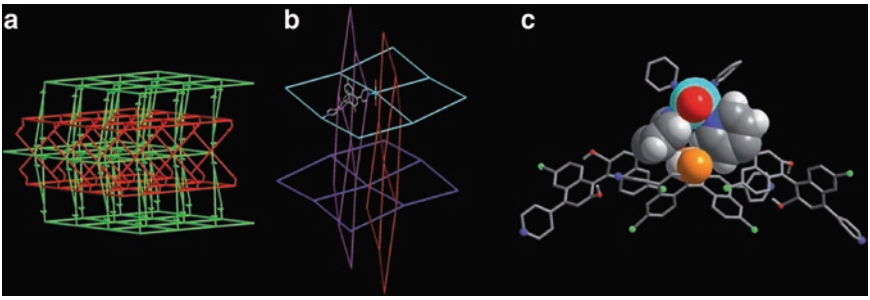

Fig. 18 (**a**) Schematic representation of the twofold interpenetration of **26**; (**b**) schematic representation of the interpenetration of mutually perpendicular 2D rhombic grids in **27**; (**c**) schematic representation of the steric congestion around the chiral dihydroxy groups of L_{25} ligands (*orange spheres*) arising from the interpenetration of 2D rhombic grids through π···π stacking interactions

26 indicated that the crystalline nature was retained after solvent removal. Moreover, CO_2 adsorption measurements showed that both evacuated samples of **26** and **27** possess permanent porosity. While **26** can effectively generate an active catalyst with Ti(Oi–Pr)$_4$ with the addition of diethylzinc to aromatic aldehydes with complete conversion and up to 90% ee, a mixture of **27** and Ti(Oi–Pr)$_4$ was not active in catalyzing the same reaction under identical conditions. The radical difference in catalytic activities of **26** and **27** was rationalized based on their different framework structures. Examination of the structure of **27** shows that the pyridyl and naphthyl rings, from mutually perpendicular interpenetrating 2D rhombic grids, form strong π···π interactions with a nearest C···C separation of 3.273 Å. As a result, all the chiral dihydroxy groups of the L_{25} ligands are tightly held in close proximity to the {Cd(py)$_2$(H$_2$O)$_2$} hinges (Fig. 18c). Due to this steric congestion, Ti(Oi–Pr)$_4$ cannot approach the binolate hydroxyl groups to form the active catalyst [91]. This observation implies that the role of the framework structure is important in determining the catalytic performance of chiral MOPMs, even if they are built from exactly the same building blocks.

A few other interesting reports on enantioselective catalysis of CMOPMs are available. Hupp and Nguyen reported an interesting CMOPM containing chiral Mn(salen) struts (salen = [(*R,R*)-(−)-1,2-cyclohexanediamino-*N,N′*-bis(3-*tert*-butyl-5-(4-pyridyl)-salicylidene)]), which was used as an asymmetric catalyst for olefin epoxidation [54]. The chiral strut, Mn^{III}(salen)Cl with (L_{28}), forms a robust pillared paddlewheel structure, $Zn_2(bpdc)_2L_{28}\cdot 10DMF\cdot 8H_2O$, **28**, which crystallizes in the triclinic P_1 space group with a 2-fold interpenetrating network (Fig. 19). The catalytic efficiency of the crystalline, porous material **28** towards the epoxidation of olefins was studied. In the presence of **28** as a catalyst and 2-(*tert*-butylsulfonyl) iodosylbenzene as an oxidant, 2,2-dimethyl-2H chromene formed the corresponding epoxide in high yield and enantioselectivity (82% ee). Slightly lower enantioselectivity than its homogeneous counterparts (88% ee) was observed, in good agreement

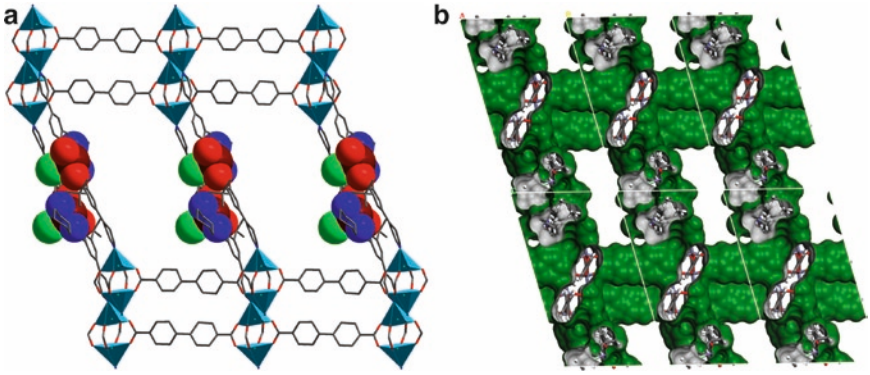

Fig. 19 (**a**) The crystal structure of the framework **28** showing interpenetrated network and framework openings; (**b**) The Connolly surface of the framework showing 2D channel structure

with the electronic effect arising from the bonded pyridyl groups to zinc cations. The compound **28** can be reused, up to third cycle (TON~1,400) with no loss of enantioselectivity and only a small loss of catalytic activity. Competitive size selectivity studies were carried out and they determined that catalysis occurs mainly in the interior and not at the surface of the catalyst. This work demonstrates that well-known salen-based Mn complexes, when confined in a CMOPM, can perform industrially important epoxidation reactions with equal efficiency as their homogeneous counterparts.

Very recently, Tanaka and coworkers have applied a copper–BINAP porous framework in the asymmetric ring opening reaction of epoxides with amines under solvent-free conditions [92]. Slow diffusion of *N,N*-dimethylaniline into a methanolic solution of (*R*)-5,5′-H_2BDA (2,2′-dihydroxy-1,1′-binaphthalene-5,5′-dicarboxylic acid, (*R*)-L_{29}) (or (*S*)-L_{29}) and $Cu(NO_3)_2$ afforded $[Cu_2(5,5'\text{-BDA})_2(H_2O)_2]\cdot MeOH\cdot 2H_2O$, (*R*)-**29**, (or (*S*)-**29**) which crystallized in a $P2_1$ space group and possessed a 2D binuclear square grid coordination network (Fig. 20). TGA of (*R*)-**29** showed 19.5% of mass loss at 25–120°C, while PXRD patterns showed reversible solvent absorption. The porous form of (*R*)-**29** is amorphous and shows catalytic activity toward asymmetric ring opening reactions of epoxides with aromatic amines. While (*S*)-BINOL was totally ineffective in catalytic ring opening reaction of epoxides, (*R*)-**29** catalyzed the reaction to afford corresponding amino alcohols in low to moderate yield with moderate enantioselectivity (40–50% ee). Although this work demonstrates for the first time, the use of Cu-based CMOPMs in epoxide ring opening reactions, the enantioselectivity is rather disappointing. There is a recent report on postsynthetic modification of a homochiral MOPM leading to a Brønsted acidic material. This material can catalyze epoxide ring opening reaction but without any asymmetric induction [93].

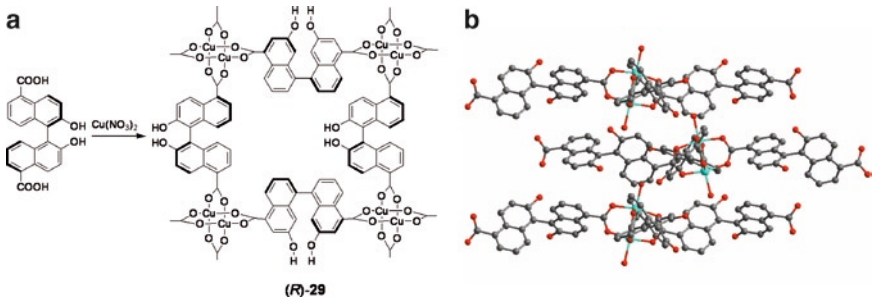

Fig. 20 (**a**) Synthesis of (*R*)-**29**; (**b**) The crystal structure of (*R*)-**29**; 2D layers are stacked in A-B-A type (viewed along the *c* axis)

Although some results described in this section are not highly exciting in terms of catalytic activity and enantioselectivity, they certainly highlight the fact that fine tunability of such a modular approach can lead to other practically useful heterogeneous asymmetric catalysts in the future.

4 Other Applications

A number of chiral coordination polymers show nonlinear optical activity and ferroelectric behavior [94–98]. The essential criterion for a compound to show either nonlinear optical activity or ferroelectric activity is that the material needs to crystallize in a noncentrosymmetric space group belonging to the polar point groups. As a chiral network itself is noncentrosymmetric, chiral coordination polymers are potentially useful as second order NLO-active materials as well as ferroelectric materials. The SHG responses of most reported chiral coordination polymers are same or less than that of urea [94–98]. However, there are a handful of examples, which show stronger SHG response. For example, $[H_2N(CH_3)_2][Zn_3(TATB)_2(HCOO)]$ (**30**) (TATB = 4,4′,4″-*s*-triazine-2,4,6-triyltribenzoate) has three times greater SHG response than urea [98]. A ferroelectric material is one that can be switched rapidly between different states by means of an external electric field. Although most of the reported ferroelectric materials are inorganic materials (e.g., KH_2PO_4, $BaTiO_3$, and $LiNbO_3$) [99], some chiral coordination polymers have also shown promising ferroelectric activity [95]. The chiral copper complex, $[Cu_2(R\text{-hmp})_2(dca)_2]$ (hmp = (*R*)-methyl-2-pyridinemethanol, dca = dicyanamide), **31**, is one such recent example [95]. However, magnetism [100–104] and photoluminescence [105,106] are two other important physical properties, which are often found in chiral coordination polymers but do not intrinsically depend on chirality of the material. It is interesting to note that often more than one of the above mentioned properties coexists in many chiral coordination polymers [94–98,105]. The reader is directed to the [107].

5 Summary and Perspectives

Since the beginning of this century, significant progress has been made in the synthesis of CMOPMs and their applications in chiral separation and catalysis. In this review article, we have discussed the strategies for the synthesis of chiral MOPMs, retaining a focus on their applications. A large number of chiral MOPMs with diverse functionalities and different topologies have been prepared mainly by two distinct approaches. The fine tunability of such approaches allows proper engineering of chiral functionalities within chiral MOPMs. With judicious choice of ligands and metal ions we can construct robust, homochiral open frameworks useful for chiral separation or heterogeneous asymmetric catalysis or both. Although still in a budding stage, CMOPMs have already shown high catalytic activity and enantioselectivity in several organic transformations such as hydrogenation of ketones and β-ketoesters, diethylzinc addition, or epoxidation. It has been established that a chiral catalyst confined inside well-organized pores can produce enantioselectivity comparable to that of its parent homogeneous catalyst. In addition, a study has revealed that the role of the framework structure is important in determining the catalytic performance of chiral MOPMs even if they are built from exactly the same building blocks. In addition, it should be pointed out that the local chirality is essential to achieve high enantioselectivity. Strategically, the synthesis of this new class of metal-organic assemblies is more controllable than the traditional immobilized catalysts and thus, this type of well-ordered, microporous materials with a high density of active catalyst centers on the surface promises to provide a new dimension in heterogeneous asymmetric catalysis. Catalyst loading, recovery, and reusability are among the important factors that determine the efficiency of a heterogeneous catalyst. So far, the preliminary results on these factors are satisfactory, but it is probably too early to raise questions regarding which of these processes have good chances of commercialization. Their ability for enantioselective sorption has been studied mostly with small chiral molecules, but several results cited in this review are still far from satisfactory. In one case, a CMOPM has been efficiently utilized as a CSP in liquid chromatography for the separation of racemates. This could well be the beginning of their potential applications in chirotechnology from a practical point of view. As a whole, the chiral MOPMs show high promise for attracting more financial and intellectual investments for potential breakthroughs in the rapidly increasing field of chirotechnology in the near future.

Note Added in Proof

Since this chapter was prepared, several important papers on the subject have been published. Wang et al. used a modified amino acid as a chiral ligand to synthesize a chiral MOPM with 1D channels (5.12×2.87 Å^2) [108]. The chiral MOPM catalyzes the addition reaction of Grignard reagent to α,β-unsaturated ketones with

excellent conversion and enantioselection. As the size of the pore is too small to accommodate the substrates, however, the catalytic reaction took place mainly on the surface of the material. Lin and coworker illustrated the synthesis of highly porous chiral MOPMs by controlling catenation through both chirality of the bridging ligands and the size of solvent molecules [109]. Bu and coworkers used a small amount of natural alkaloids, (–)-cinchonidine or (+)-cinchonine, to induce the homochiral crystallization of a chiral framework constructed from achiral components [110]. Unlike typical chiral templates, these alkaloids catalytically induced the bulk homochirality without incorporating themselves into the framework. Kim and coworkers have successfully employed the post-modification approach to synthesize catalytically active chiral MOPMs using a pre-assembled robust 3D framework, MIL-101, and chiral catalytic organic units [111]. L-Proline-based chiral organic ligands were incorporated at the unsaturated Cr(III) centers of MIL-101 keeping the parent framework intact. The new chiral MOPMs showed remarkable catalytic activities in asymmetric aldol reactions (yield up to 90% and ee up to 80%), including much higher enantioselectivity than the corresponding chiral catalytic organic units as homogeneous catalysts.

Acknowledgment We gratefully acknowledge the Creative Research Initiatives, Brain Korea 21, and World Class University (WCU) (Project No. R31-2008-000-10059-0) programs of the Korean Ministry of Education, Science and Technology (MOEST), and the Steel Science Programs of POSCO for support of this work.

References

1. Corma A (1997) Chem Rev 97:2373
2. Maesen TLM, Marcus B (2001) In: van Bekkum H, Flanigen EM, Jacobs PA, Jansen JC (eds) Introduction to zeolite science and practice. Elsevier, Amsterdam, p 1
3. Song CE, Lee SG (2002) Chem Rev 102:3495
4. Newsam JM, Treacy MMJ, Koetsier WT, de Gruyter CB (1988) Proc R Soc Lond Ser A 420:375
5. Anderson MW, Terasaki O, Ohsuna T, Philippou A, MacKay SP, Ferreira A, Rocha J, Lidin S (1994) Nature 367:347
6. Janiak C (2003) Dalton Trans:2781
7. James SL (2003) Chem Soc Rev 32:276
8. Rosseinsky MJ (2004) Microporus Mesoporous Mater 73:15
9. Rowsell JLC, Yaghi OM (2005) Angew Chem Int Ed 44:4670
10. Férey G (2008) Chem Soc Rev 37:191
11. Morris RE, Wheatley PS (2008) Angew Chem Int Ed 47:4966
12. Lin W (2005) J Solid State Chem 178:2486
13. Lin W (2005) Top Catal 34:85
14. Lin W (2007) MRS Bull 32:544
15. Wells AF (1977) Three-dimensional nets and polyhedra. Wiley, New York
16. Janiak C (1997) Angew Chem Int Ed Engl 36:1431
17. Kondo M, Okubo T, Asami A, Noro SI, Yoshitomi T, Kitagawa S, Ishii T, Matsuzaka H, Seki K (1999) Angew Chem Int Ed 38:140
18. Moulton B, Zaworotko MJ (2001) Chem Rev 101:1629 and references therein

19. Khlobystov AN, Blake AJ, Champness NR, Lemenovskii DA, Majouga AG, Zyk NV, Schröder M (2001) Coord Chem Rev 222:155
20. Barnett SA, Champness NR (2003) Coord Chem Rev 246:145
21. Desiraju GR (1989) Crystal engineering. The design of organic solids. Elsevier, Amsterdam
22. Desiraju GR (2002) Acc Chem Res 35:565 and references therein
23. Steiner T (2002) Angew Chem Int Ed 41:48
24. Hoskins BF, Robson R (1990) J Am Chem Soc 112:1546
25. Biradha K, Seward C, Zaworotko MJ (1999) Angew Chem Int Ed 38:492
26. Zaworotko MJ (2000) Angew Chem Int Ed 39:3052
27. Yaghi OM, Li H, Davis C, Richardson D, Groy TL (1998) Acc Chem Res 31:474
28. Eddaoudi M, Moler DB, Li H, Chen B, Reineke TM, O'Keeffe M, Yaghi OM (2001) Acc Chem Res 34:319
29. Wang Z, Kravtsov VC, Zaworotko MJ (2005) Angew Chem Int Ed 44:2877
30. Eddaoudi M, Kim J, Rosi N, Vodak D, O'Keeffe M, Yaghi OM (2002) Science 295:469
31. Yaghi OM, O'Keeffe M, Ockwig N, Chae HK, Eddaoudi M, Kim J (2003) Nature 423:705
32. Ockwig N, Friedrichs OD, O'Keeffe M, Yaghi OM (2005) Acc Chem Res 38:176
33. Zhang JP, Lin YY, Huang XC, Chen XM (2005) J Am Chem Soc 127:5495
34. Evans OR, Lin W (2002) Acc Chem Res 35:511
35. Halder GJ, Kepert CJ, Moubaraki B, Murray KS, Cashion JD (2002) Science 298:1762
36. Dincă M, Long JR (2007) J Am Chem Soc 129:11172
37. Noro S, Kitagawa S, Kondo M, Seki K (2000) Angew Chem Int Ed 39:2081
38. Rosi NL, Eckert J, Eddaoidi M, Vodak DT, Kim J, O'Keeffe M, Yaghi OM (2003) Science 300:1127
39. Kitagawa S, Kitaura R, Noro S (2004) Angew Chem Int Ed 43:2334
40. Fujita M, Kwon YJ, Washizu S, Ogura K (1994) J Am Chem Soc 116:1151
41. Seo JS, Whang D, Lee H, Jun SI, Oh J, Jeon Y, Kim K (2000) Nature 404:982
42. Joy A, Ramamurthy V (2000) Chem Eur J 6:1287
43. Sivasubramanian K, Kaanumalle LS, Uppili S, Ramamurthy V (2007) Org Biomol Chem 5:1569
44. Withersby MA, Blake AJ, Champness NR, Hubberstey P, Li WS, Schröder M (1997) Angew Chem Int Ed Engl 36:2327
45. Batten SR, Hoskins BF, Robson R (1997) Angew Chem Int Ed Engl 36:636
46. Krämer R, Lehn JM, De Cian A, Fischer J (1993) Angew Chem Int Ed Engl 32:703
47. Chen XD, Du M, Mak TCW (2005) Chem Commun:4417
48. Abrahams BF, Jackson PA, Robson R (1998) Angew Chem Int Ed 37:2656
49. Kepert CJ, Rosseinsky MJ (1998) Chem Commun:31
50. Kepert CJ, Prior TJ, Rosseinsky MJ (2000) J Am Chem Soc 122:5158
51. Lin Z, Slawin AMZ, Morris RE (2007) J Am Chem Soc 129:4880
52. Ranford JD, Vittal JJ, Wu D (1998) Angew Chem Int Ed 37:1114
53. Kesanli B, Cui Y, Smith MR, Bittner EW, Bockrath BC, Lin W (2005) Angew Chem Int Ed 44:72
54. Cho SH, Ma B, Nguyen ST, Hupp JT, Albrecht-Schmitt TE (2006) Chem Commun:2563
55. Zhang J, Liu R, Feng P, Bu X (2007) Angew Chem Int Ed 46:8388
56. Dybtsev DN, Nuzhdin AL, Chun H, Bryliakov KP, Talsi EP, Fedin VP, Kim K (2006) Angew Chem Int Ed 45:916
57. Vaidhyanathan R, Bradshaw D, Rebilly JN, Barrio JP, Gould JA, Berry NG, Rosseinsky MJ (2006) Angew Chem Int Ed 45:6495
58. Hasegawa S, Horike S, Matsuda R, Furukawa S, Mochizuki K, Kinoshita Y, Kitagawa S (2007) J Am Chem Soc 129:2607
59. Wang Z, Cohen SM (2007) J Am Chem Soc 129:12368
60. Tanabe KK, Wang Z, Cohen SM (2008) J Am Chem Soc 130:8508
61. Hwang YK, Hong DY, Chang JS, Jhung SH, Seo YK, Kim J, Vimont A, Daturi M, Serre C, Férey G (2008) Angew Chem Int Ed 47:4144
62. Collins AN, Sheldrake GN, Crosby J (1996) Chirality in industry. Wiley, NY

63. Blaser HU, Spindler F, Studer M (2001) Appl Catal A Gen 221:119
64. Oehme G (1999) In: Jacobsen EN, Pfaltz A, Yamamoto H (eds) Comprehensive Asymmetric Catalysis. Springer-Verlag, Berlin, Vol 3, p 1378
65. Heitbaum M, Glorius F, Escher I (2006) Angew Chem Int Ed 45:4732
66. McMorn P, Hutchings GJ (2004) Chem Soc Rev 33:108
67. Sherrington DC (2000) Catal Today 57:87
68. Ding K, Wang Z, Wang X, Liang Y, Wang X (2006) Chem Eur J 12:5188
69. Pini D, Mandoli A, Orlandi S, Salvadori P (1999) Tetrahedron Asymmetry 10:3883
70. Ward TJ (2006) Anal Chem 78:3947
71. Maier NM, Lindner W (2007) Anal Bioanal Chem 389:377
72. Gübitz G, Martin G, Schmid MG (2007) Electrophoresis 28:114
73. Cancelliere G, D'Acquarica I, Gasparrini F, Maggini M, Misiti D, Villani C (2006) J Sep Sci 29:770
74. Xiong RG, You XZ, Abrahams BF, Xue ZL, Che CM (2001) Angew Chem Int Ed 40:4422
75. Xie YR, Wang XS, Zhao H, Zhang J, Weng LH, Duan CY, Xiong RG, You XZ, Xue ZL (2003) Organometallics 22:4396
76. Song YM, Zhou T, Wang XS, Li XN, Xiong RG (2006) Cryst Growth Des 6:14
77. Bradshaw D, Prior TJ, Cussen EJ, Claridge JB, Rosseinsky MJ (2004) J Am Chem Soc 126:6106
78. Nuzhdin AL, Dybtsev DN, Bryliakov KP, Talsi EP, Fedin VP (2007) J Am Chem Soc 129:12958
79. Muppidi VK, Zacharias PS, Pal S (2005) Chem Commun:2515
80. Muppidi VK, Zacharias PS, Pal S (2007) J Solid State Chem 180:132
81. Sawaki T, Dewa T, Aoyama Y (1998) J Am Chem Soc 120:8539
82. Gao Y, Wada T, Yang K, Kim K, Inoue Y (2005) Chirality 17:S19
83. Evans OR, Ngo HL, Lin W (2001) J Am Chem Soc 123:10395
84. Hu A, Ngo HL, Lin W (2003) Angew Chem Int Ed 42:6000
85. Hu A, Ngo HL, Lin W (2003) J Am Chem Soc 125:11490
86. Ngo HL, Hu A, Lin W (2004) J Mol Catal A Chem 215:177
87. Wu CD, Hu A, Zhang L, Lin W (2005) J Am Chem Soc 127:8940
88. Wu CD, Lin W (2007) Angew Chem Int Ed 46:1075
89. Ohkuma T, Ooka H, Ikariya T, Noyori R (1995) J Am Chem Soc 117:10417
90. Doucet H, Ohkuma T, Murata K, Yokozawa T, Kozawa M, Katayama E, England AF, Ikariya T, Noyori R (1998) Angew Chem Int Ed 37:1703
91. Jiang H, Lin W (2004) Org Lett 6:861
92. Tanaka K, Oda S, Shiro M (2008) Chem Commun:820
93. Ingleson MJ, Barrio JP, Bacsa J, Dickinson C, Park H, Rosseinsky MJ (2008) Chem Commun:1287
94. Gu ZG, Zhou XH, Jin YB, Xiong RG, Zuo JL, You XZ (2007) Inorg Chem 46:5462
95. Zang S, Su Y, Li Y, Ni Z, Meng Q (2006) Inorg Chem 45:174
96. Xie YR, Zhao H, Wang XS, Qu ZR, Xiong RG, Xue X, Xue Z, You XZ (2003) Eur J Inorg Chem 3712
97. Zang S, Su Y, Li Y, Zhu H, Meng Q (2006) Inorg Chem 45:2972
98. Sun D, Ke Y, Collins DJ, Lorigan GA, Zhou HC (2007) Inorg Chem 46:2725
99. Lee HN, Christen HM, Chisholm MF, Rouleau CM, Lowndes DH (2005) Nature 433:395
100. Gao EQ, Yue YF, Bai SQ, He Z, Yan CH (2004) J Am Chem Soc 126:1419
101. Inoue K, Kikuchi K, Ohba M, Okawa H (2003) Angew Chem Int Ed 42:4810
102. Imai H, Inoue K, Kikuchi K, Yoshida Y, Ito M, Sunahara T, Onaka S (2004) Angew Chem Int Ed 43:5618
103. Wen HR, Wang CF, Song Y, Zuo JL, You XZ (2005) Inorg Chem 44:9039
104. Liu WL, Song Y, Li YZ, Zou Y, Dang DB, Ni CL, Meng QJ (2004) Chem Commun:2348
105. Wang L, Yang M, Li G, Shi Z, Feng S (2006) Inorg Chem 45:2474
106. Yue Q, Yang J, Li GH, Li GD, Chen JS (2006) Inorg Chem 45:4431

107. Roques N, Mugnaini V, Veciana J (2009) Magnetic and porous molecule-based materials. Top Curr Chem . doi:10.1007/128_2009_8
108. Wang M, Xie MH, Wu CD, Wang YG (2009) Chem Commun:2396
109. Ma L, Lin W (2008) J Am Chem Soc 130:13834
110. Zhang J, Chen S, Wu T, Feng P, Bu X (2008) J Am Chem Soc 130:12882
111. Banerjee M, Das S, Yoon M, Choi HJ, Hyun MH, Park SM, Seo G, Kim K (2009) J Am Chem Soc 131:7524